arXiv:1006.0335v1 [astro-ph.HE] 2 Jun 2010

X-ray Counterparts of Millisecond Pulsars in Globular Clusters

W. Becker[1], H.H. Huang[1], T. Prinz[1]

ABSTRACT

We have systematically studied the X-ray emission properties of globular cluster millisecond pulsars in order to evaluate their spectral properties and luminosities in a uniform way. Cross-correlating the radio timing positions of the cluster pulsars with the high resolution Chandra images revealed 31 X-ray counterparts identified in nine different globular cluster systems, including those in 47 Tuc. Timing analysis has been performed for all sources corresponding to the temporal resolution available in the archival Chandra data. Making use of unpublished data on M28, M4 and NGC 6752 allowed us to obtain further constraints for the millisecond pulsar counterparts located in these clusters. Counting rate and energy flux upper limits were computed for those 36 pulsars for which no X-ray counterparts could be detected. Comparing the X-ray and radio pulse profiles of PSR J1821-2452 in M28 and the 47 Tuc pulsars PSR J0024-7204D,O,R indicated some correspondence between both wavebands. The X-ray efficiency of the globular cluster millisecond pulsars was found to be in good agreement with the efficiency $L_X \sim 10^{-3}\dot{E}$ observed in Galactic field rotation-powered pulsars. Millisecond pulsars in the galactic plane and in globular clusters appear to show no distinct differences in their X-ray emission properties.

Subject headings: globular clusters:general — globular clusters:individual (Terzan 5, 47 Tucanea, NGC 104, M28, NGC 6626, M15, NGC 7078, NGC 6440, M62, NGC 6266, NGC 6752, M3, NGC 5272, M5, NGC 5904, M13, NGC 6205, NGC 6441 M22, NGC 6656, M30, NGC 7099, NGC 6544, M4, NGC 6121, M53, NGC 5024, M71, NGC 6838, NGC 6397) — stars:neutron — x-ray:stars — binaries:general — pulsars:general — pulsars:individual (PSR J0024-7204C, J0024-7204D, J0024-7204E, J0024-7204F, J0024-7204G, J0024-7204H, J0024-7204I, J0024-7204J, J0024-7204L, J0024-7204M, J0024-7204N, J0024-7204O, J0024-7204Q, J0024-7204R, J0024-7204S, J0024-7204T, J0024-7204U, J0024-7204W, J0024-7204Y, J1824-2452A, J1824-2452G, J1824-2452H, J1748-2021B, J1701-3006B, J1701-3006B, J1701-3006C, J1911-6000C, J1910-5959D, B1620-26, J1953+1846A , J1748-2446, J1740-5340, J1748-2021A, J1748-2021C, J1748-2021D, J1748-2021E, J1748-2021F, J1750-3703A, J1750-3703B,

---

[1] Max-Planck Institut für Extraterrestrische Physik, 85741 Garching bei München, Germany

J1750-3703C, J1750-3703D, J1807-2459A, J1910-5959B, J1910-5959E, J1641+3627A, B2127+11A, B2127+11B, B2127+11C, B2127+11D, B2127+11E, B2127+11F, B2127+11G, B2127+11H, J1824-2452B, J1824-2452C, J1824-2452D, J1824-2452E, J1824-2452F, J1824-2452I, J1824-2452J, J2140-2310A, J1342+2822B, J1342+2822D, B1516+02A, B1516+02B, J1701-3006A, J1748-2446A, J1748-2446C)

1. INTRODUCTION

In recent years it became obvious that globular clusters (GCs) are millisecond pulsar factories. Their high stellar density along with a frequent dynamical interaction of cluster constituents provides an efficient environment for the formation of short-period (binary) pulsars (Rasio 2000; Fregeau 2008; Ivanova 2008). Extensive surveys using telescopes with increasing sensitivity kept the radio population of cluster pulsars persistently growing (Camilo & Rasio 2005; Ranson 2008). As of spring 2010 about 160 ($\sim$ 9%) of the 1864 cataloged radio pulsars fall under the category of millisecond pulsars, i.e. are recycled Manchester & Hobbs (2005). 140 ($\sim$ 87%) of them are located in 26 GCs[2]. Of these globular cluster millisecond pulsars 59 ($\sim$ 42%) appear to be solitary, the others are in binaries. The formation scenario of solitary recycled pulsars is still under discussion, but it is widely believed that the pulsar's companion either gets evaporated (a process which is believed to be at work e.g. in the PSR B1957+20 millisecond pulsar/binary system) or that the system gets tidally disrupted after the formation of the millisecond pulsar. Whatever the mechanism is, it is interesting to note that the ratio of solitary to binary millisecond pulsars in globular clusters is almost identical to the 40% observed in the population of galactic disk millisecond pulsars (cf. Becker 2009). Figure 1 illustrates the cataloged distribution of X-ray and radio millisecond pulsars in each of the 26 globular clusters known to host millisecond pulsars.

The first millisecond pulsar found in a globular cluster was PSR J1824-2452A (Lyne et al. 1987) which is located in NGC 6626 (M28). PSR J1824-2452A is not only the youngest ($P/2\dot{P} = 3.0 \times 10^7$ yrs) but also the most powerful ($\dot{E} = 2.24 \times 10^{36} I_{45}$ erg s^{-1}) and brightest X-ray pulsar in a globular cluster. X-ray emission from it was first detected in ROSAT HRI data (Danner et al. 1997). With an angular resolution of $\sim$ 5" (HEW) the HRI, though, did not fully allow to resolve its emission into a point source. It therefore was unclear whether the pulsar powers a plerion or its X-ray emission was partly due to a superposition of multiple discrete cluster sources surrounding it. Today we know that sub-arcsecond spatial resolution is required to adequately study globular cluster sources in the X-ray band. Chandra resolved PSR J1824-2452A into a point source along with 12 other X-ray sources surrounding it within the cluster's $0'.24$ core radius (Becker et al. 2003). Apparently they are the cause of the diffuse X-ray emission seen to surround PSR J1824-2452A in the ROSAT HRI data.

---

[2] http://www.naic.edu/$\sim$pfreire/GCpsr.html

PSR J1824-2452A is a strong non-thermal X-ray emitter (cf. Becker et al. 2003, see also Table 6.7 in Becker 2009 for a summary of spectral parameters from X-ray detected millisecond pulsars). It has a relatively hard X-ray spectrum, so that X-ray pulses could be detected up to ~ 20 keV with the Rossi X-ray Timing Explorer (Mineo et al. 2004). The X-ray pulse profile is characterized by narrow peaks and small features with a high fraction of pulsed photons (Saito et al. 1997; Becker & Trümper 1999; Rutledge et al. 2004). As thermal emission can not be beamed strong enough to explain the narrow pulse peaks and high pulsed fraction, both the spectral and temporal emission properties are in agreement with the interpretation that its X-ray emission is caused by non-thermal radiation processes in the pulsar's magnetosphere.

This is similar to what is observed in some other galactic plane millisecond pulsars (Becker 2009; Zavlin 2007; Becker & Trümper 1999). However, the data quality available from all those pulsars is far from being homogenous. Whereas from several of these sources high quality spectral, temporal and spatial information is available, for many others, especially those in globular clusters, the photon statistics is small. This is especially true for most of the pulsars seen in 47 Tuc. For this cluster Grindlay et al. (2001) reported the detection of 108 sources within a region corresponding to about 5 times the 47 Tuc core radius ($r_{core} \sim 115$ arcsec). Nineteen of the soft/faint sources were found to be positionally coincident with millisecond radio pulsars. Most turned out to have a soft X-ray spectrum (Bogdanov et al. 2006) and an X-ray luminosity in the range $L_X \sim 10^{30} - 10^{31}$ ergs s^{-1}, which is about two to three orders of magnitudes smaller than that of PSR J1824-2452A. According to Grindlay et al. (2001) more than fifty percent of the unidentified sources in 47 Tuc could be millisecond pulsars.

Gamma-ray emission from millisecond pulsars was detected by the Fermi Large Area Telescope recently (Abdo et al. 2009a,b). Because of the large population of millisecond pulsars in globular clusters eight of them have been detected meanwhile as steady point-like high-energy gamma-ray sources (Abdo et al. 2010), including 47 Tuc (Webb & Knödlseder 2010).

As demonstrated by the examples above, the brightness and hardness of globular cluster pulsars spans a very wide range. Of the 140 cluster millisecond pulsars known today only few are found to have an X-ray counterpart. To increase this sample and to study their emission properties more systematically is the motivation for this paper. The structure is as follows: in §2 we describe the source detection and identification along with the spectral and timing analysis of the detected millisecond pulsar counterparts. Their emission properties compared to those observed in Galactic plane millisecond pulsars are discussed in §3.

2. OBSERVATIONS AND DATA REDUCTION

A decade after the launch of Chandra 18 out of the 26 globular clusters which are known to host millisecond pulsars were observed with the ACIS and/or HRC detector in focus. We made use of all data publicly available by spring 2010. For counterpart searches and/or spectral analysis there are 45 ACIS-S/I and 5 HRC-I observations available, summing up to a total of 1.566,419 ksec and 52.442 ksec of good data. HRC-S data with the timing-option enabled are available for 47 Tuc and M28, summing up to a total of 792,620 ksec and 90,440 ksec, respectively. The corresponding observational details of these datasets are summarized in Table 1. Distance, half-mass radius and column density of the globular clusters which are known to host millisecond pulsars are summarized in Table 2. The basic pulsar parameters for all millisecond pulsars considered in this work are summarized in Tables 3 and 4. Although several of them have been previously analyzed by various authors, leading to proposed counterpart assignments for some of the millisecond pulsars, new and so far unpublished data were available for NGC 6626 (M28), NGC 6266 (M4) and NGC 6752.

Standard processed level-2 data were used in all counterpart searches. Prior to the data analysis, aspect offsets for each observation, which is a function of the spacecraft roll angle, was carefully checked and corrected. The data analysis was restricted to the $0.3-8$ keV energy range.

2.1. SOURCE DETECTION AND IDENTIFICATION

To search for X-ray counterparts in the available datasets we used the WAVELET and CELDETECT algorithms as implemented in the CIAO 4.2 software package. Source positions were then correlated with the radio timing positions of the globular cluster millisecond pulsars. To assess all identifications we computed the probability for a chance coincidence according to $P_{coin} = (N_X^{\rm all}/r_{\rm s}^2)\ \delta{\rm RA}\ \delta{\rm Dec}$. Here $N_X^{\rm all}$ is the number of X-ray sources detected within a search region of radius $r_{\rm s}$ and δRA δDec are the positional uncertainties in right ascension and declination. The latter was determined by combining the errors of the radio pulsar and X-ray source positions in quadrature, considering Chandra's absolute astrometric accuracy to be $0.21''$. This astrometric accuracy was estimated from the distribution of aspect offsets for a sample of point sources with accurately known celestial positions[3]. There are 68% of 237 sources imaged with ACIS-S which have offsets smaller than or equal to $\sim 0.21''$. As all the data used for counterpart searches were taken with the ACIS-S we included this value in our error budget computation for each coordinate. For the search radius $r_{\rm s}$ we used the globular cluster half-mass radius as most of the pulsars lie within this region. The pulsar PSR J1911 – 6000C in NGC 6752, though, is located outside this radius so that we expanded the search region for this cluster to 3 arcmin. The resulting identifications, counting rates and chance probabilities for finding an X-ray source by chance at the radio pulsar position are listed in Table 5.

---

[3] See http://cxc.harvard.edu/cal/ASPECT/celmon/ for details

In total 31 X-ray sources in nine globular clusters were found to be coincident with the radio timing position of known millisecond pulsars. Among them are the 19 millisecond pulsars previously identified in 47 Tuc (Grindlay et al. 2001; Bogdanov et al. 2006), the millisecond pulsar PSR J1824-2452A in NGC 6626 (Becker et al. 2003), PSR 1953+1846A in NGC 6838 (Elsner et al. 2008), PSR J1701-3006B in NGC 6266 (Cocozza et al. 2008), PSR J1740-5340 in NGC 6397 (Huang & Becker 2010) and few more for which an association has been assigned in the literature (cf. Table 6.9 in Becker 2009 and references therein). Pulsars for which X-ray counterparts are newly detected are PSR J1824-2452G and PSR J1824-2452H in NGC 6626 and PSR J1701-3006C in NGC 6266. The tentative assignment of the X-ray counterparts for PSR J2140-3310A in M30 (Ransom et al. 2004) and PSR J1910-5959B (D'Amico et al. 2002) could not be confirmed by our analysis, albeit additional data were available for the latter pulsar compared to their analysis.

Counting rate upper limits were computed for those pulsars for which no X-ray counterpart could be detected. For this we measured the number of counts recorded at the radio pulsar position and computed the 3σ upper limits according to $C_{3\sigma} = 0.5 \times (S/N)^2 + (S/N) \times \sqrt{cts + 0.25 \times (S/N)^2}$. Here $S/N = 3$ is the signal-to-noise ratio and cts the counts obtained within a circle of 1 arcsec radius centered on the position of the radio pulsar. All upper limits are summarized in Table 6 along with the exposure time of the observation and the number of counts recorded at the pulsar position. Figures 2 to 10 show ACIS-S and/or HRC-I images of all globular clusters considered in this work. The location of the millisecond pulsars and the cluster half-mass radius are indicated.

2.2. TIMING ANALYSIS AND SEARCHES FOR LONG TERM FLUX VARIABILITY

2.2.1. THE GLOBULAR CLUSTER X-RAY PULSARS

For about ten years the 3.05 ms pulsar PSR J1824-2452A in M28 was the only globular cluster pulsar from which pulsed X-ray emission had been detected. Timing observations were performed with ROSAT (Danner et al. 1997), ASCA (Saito et al. 1997), BeppoSax (Mineo et al. 2004) and the Rossi X-ray Timing Explorer (e.g. Rots 2006). XMM-Newton lists the pulsar as calibration target, although it was never scheduled for observations so far. Chandra observed PSR J1824-2452A in 2002 and 2006 for a total of $\sim 90,440$ ksec using the HRC-S with the timing flag enabled. The temporal resolution of the HRC-S in this mode is $15.625\,\mu s$. It is sensitive in the

$0.08-10$ keV band[4]. The intrinsic energy resolution of the HRC being a channel plate detector is marginal. Rutledge et al. (2004) used the 2002 data together with a series of archival XTE data to re-investigate the pulsars temporal X-ray emission properties. With respect to their analysis we included the HRC-S observation taken in 2006 which almost doubles the number of photons available for the Chandra timing analysis of PSR J1824-2452A. This allowed us to measure the pulse arrival time, fraction of pulsed photons, the width of the two X-ray pulses and the pulse phase separation of the two peaks by using the Chandra data alone. As Chandra is an imaging instrument it allows to measure the pulse properties by its better signal-to-noise ratio with much higher accuracy than using XTE data only.

Selecting all events from within a circle of 1.5 arcsec radius centered on the pulsar position gave us a total of 773 counts to construct a pulse profile by period folding (Buccheri & De Jager 1989). The background contribution is estimated to be 45 ± 7 counts. The pulsar ephemeris which were used to fold the arrival times with the pulsar's rotation period P=3.0543151 ms, predicted for the epoch JD=2451468.5, are summarized in Table 7. The X-ray pulse profile relative to the radio profile taken at 800 MHz by Backer & Sallmen (1997) is shown in Figure 11. Unlike the radio profile, which is observed to show three peaks of which the second is observed to vary in intensity on time scales of weeks to month (Backer & Sallmen 1997), only two narrow pulse peaks are observed in the X-ray band. Their phase separation obtained from fitting the pulse peaks by Gaussian functions is found to be 0.449 ± 0.0009. The FWHM of the phase width of the first and second peaks are fitted to be 0.0273 ± 0.0009 and 0.053 ± 0.002, corresponding to 9.8 ± 0.3 and 19.3 ± 0.7 degrees. The three radio pulse peaks have a phase separation of $\mathrm{RP2}-\mathrm{RP1} = 0.295 \pm 0.001$ and $\mathrm{RP3}-\mathrm{RP2} = 0.193 \pm 0.003$. The FWHM phase width of the radio pulse peaks are fitted to be 0.0452 ± 0.0013, 0.037 ± 0.002 and 0.16 ± 0.01 for the main, second and third radio pulse. The X-ray pulsed fraction is determined to be 85 ± 4% by using a bootstrap method (cf. Becker & Trümper 1999; Swanepoel et al. 1996). The error represents the 1σ confidence range. For the phase difference between the radio and X-ray peak it can be seen from Figure 11 that the main radio pulse leads the main X-ray pulse by 0.0243 ± 0.0004 in phase, corresponding to $74.2 \pm 1.2\,\mu$s. Rots (2006) has recently estimated the accuracy of Chandra's absolute time stamps to be $4 \pm 4\,\mu$s. A 3σ clock uncertainty of $16\,\mu$s together with the HRC's intrinsic temporal resolution thus results in a total uncertainty of $32\,\mu$s for the absolute phase assigned to an X-ray photon. Using 79 phase bins to construct the X-ray profile one bin corresponds to $\sim 38\,\mu$s of the pulsar's rotation period. The uncertainty of the relative phase between the radio and X-ray profiles plotted in Figure 11 thus corresponds to ± 1 phase bin in the X-ray profile.

The only other globular cluster millisecond pulsars for which pulsed X-ray emission is detected are located in 47 Tuc. So far, $\sim$ 800 ksec deep Chandra observations found X-ray pulses from only three of the nineteen 47 Tuc millisecond pulsars (Cameron et al. 2007). We used the archival HRC-S data (cf. Table 1) to re-analyze these data in order to consistently determine their temporal emission properties. The ephemeris we used are summarized in Table 7. X-ray pulses are reported for PSR J0024-7204D, PSR J0024-7204O and PSR J0024-7204R. PSR J0024-7204D is a solitary pulsar spinning at a period of 5.35 ms. PSRs J0024-7204 O,R are in short-period binaries (Camilo et al. 2000) with a ~ 0.02 $M_\odot$ companion. Their spin / orbit periods are 2.64 ms / 3.26 h and 3.48 ms / 1.58 h, respectively. For analyzing their temporal emission properties we selected all events from circular regions of radius 1 arcsec or 1.5 arcsec, centered on the pulsar position. The smaller selection radius was used for J0024-7204 O,R in order to minimize a possible flux contribution from neighboring sources located in the crowded cluster center (cf. Figure 2). The barycentered photon arrival times were coherently folded with the spin-period extrapolated to the epoch t_0 listed in Table 7. The z_n^2-test (Buccheri & De Jager 1989) was applied for $n = 1 - 10$ harmonics in combination with the H-test (de Jager 1987) to determine the significance of the pulsed signal as a function of its harmonic content. According to this tests the pulsations in PSR J0024-7204 D,R have the highest significance of 3.64σ, and 3.96σ for $n = 2$ harmonics whereas the pulsed signal in J0024-7204O is found to have a significance of 4.84σ for $n = 3$ harmonics. The pulse profiles are shown in Figure 12. They all appear to be double peaked with a phase separation of 0.44 ± 0.06, 0.50 ± 0.02 and 0.4 ± 0.04 for PSRs J0024-7204 D,O,R. The phase width of the two peaks are 0.4 ± 0.1 (FWHM) and 0.25 ± 0.15 (FWHM) for PSR J0024-7204 D, 0.15 ± 0.04 (FWHM) and 0.27 ± 0.02 (FWHM) for PSR J0024-7204 O and 0.2 ± 0.06 (FWHM) and 0.32 ± 0.05 (FWHM) for PSR J0024-7204R. For the fraction of pulsed photons we measured $60 \pm 15\%$ for PSR J0024–7204 D, $57 \pm 15\%$ for PSR J0024–7204 O and $64 \pm 17\%$ for PSR J0024–7204 R using a bootstrap method (cf. Becker & Trümper 1999; Swanepoel et al. 1996). Figure 13 shows the pulsar's X-ray profiles together with their corresponding radio profiles observed at 1400 MHz by Freire et al. (2010, in prep.).

---

[4] http://hea-www.harvard.edu/HRC/overview/overview.html

2.2.2. *SEARCHES FOR LONG TERM FLUX VARIABILITY*

The 3.2 s frame time of the ACIS-S detector does not allow to search for coherent X-ray pulsations from the clusters' millisecond pulsars. Most of the sources considered in this work, though, were in the focus of the ACIS-S for multiple times, permitting us to investigate their temporal behavior on longer time scales. The length of the time scales in the various datasets is given by the time gaps between the different observations, e.g. hours to years.

We checked the counting rates of all pulsars for variability (cf. Table 5). Binary pulsars (cf. Table 3) were tested on whether they show flux variability related to e.g. their orbital binary motion. This was observed in 47 Tuc W (Bogdanov et al. 2005) which exhibits large-amplitude X-ray variability, probably due to geometric occultations of an X-ray emitting intra-binary shock by the companion main-sequence star (Bogdanov et al. 2006). As an example, Figure 14 shows the lightcurves of the M28 pulsars PSR J1824-2452G and J1824-2452H as folded at their binary period. PSR J1824-2452G is in a 2.51 h binary system with a low-mass companion. J1824-2452H has an orbit period of 10.87 h and has been observed to show radio eclipses (Bégin 2006). Indeed, inspecting the lightcurves by eye may reveal a flux variability with the pulsar's orbital binary motion. From the statistical point of view, though, the significance for variability depends on the number of phase bins and is only at the $\sim 1.5-2\sigma$ level for lightcurves with 6, 8 or 10 phase bins.

More stringent results were found for PSR J1748-2021B in NGC 6440 and for PSR J1740-5340 in NGC 6397. PSR J1748-2021B has an orbital period of $\sim$ 20 days (Freire et al. 2008). It was observed by Chandra twice, in 2000 July 4 and three years later in 2003 June 27. These observations cover the relatively narrow orbital phase intervals[5] $0.124-0.137$ and $0.058-0.072$. The vignetting corrected net counting rates which we have measured from the pulsar in this two datasets are $(1.68\pm0.28)\times10^{-3}$ cts/s and $(5.03\pm0.46)\times10^{-3}$ cts/s, respectively. The counting rates measured in both data thus differ by a factor of ~ 3 with a significance of $\sim 6\sigma$. On whether this variability is because of a modulation of the X-ray flux over the pulsar's binary orbit or because of a long term flux increase by other means can not be clarified with the available data.

The millisecond pulsar PSR J1740-5340 in NGC 6397 is in a ~ 1.35 day binary orbit with a massive late type companion. The pulsar's radio emission is seen to eclipse in the orbital phase interval $0.05-0.45$ (D'Amico et al. 2001). Five datasets from NGC 6397 are available in the Chandra archive (cf. Table 1), covering various phase ranges of the pulsar's binary orbit (see Huang & Becker 2010 for a more detailed discussion). The first observation done in 2000 July 31 was aimed on the front-illuminated (FI) ACIS-I3 chip, while the other four observations were taken with the back-illuminated (BI) chip ACIS-S3. The pulsar's net counting rates obtained from this data are $(1.31\pm0.17)\times10^{-3}$ cts/s, $(1.74\pm0.25)\times10^{-3}$ cts/s, $(2.89\pm0.33)\times10^{-3}$ cts/s, $(2.26\pm0.16)\times10^{-3}$ cts/s and $(2.92\pm0.14)\times10^{-3}$ cts/s, respectively, revealing a $\sim 3\sigma$ flux variability on time scales of month to years. Figure 15 shows the pulsar lightcurve as folded at the binary period. The significance of the flux modulation over the observed orbit was found to be between 88.5% and 99,6%, depending on the number of phase bins used to construct the lightcurve (cf. Huang & Becker 2010).

---

[5] The zero point is set to the ascending node.

2.3. SPECTRAL ANALYSIS

The ACIS-S CCDs provide spectral information for all cluster pulsars for which counterparts are detected. The quality of spectral fits and the constraint on the parameters of the model-spectra, however, is a function of photon statistics and thus varies significantly among the detected counterparts. In addition, the column absorption towards the various globular clusters shows a large diversity (cf. Table 2), meaning that the sensitivity to detect soft X-rays from e.g. thermal hotspots on the neutron star surface may be higher for some clusters (e.g. in 47 Tuc) than in others (e.g. Terzan 5).

The extraction of the source and background spectra as well as the computation of the corresponding response and effective area files were performed with the data reduction package CIAO 4.2 by using the calibration data in CALDB 4.2. To extract the spectra we used circular regions of $2''$ radius (corresponding to $\sim 95\%$ encircled energy) centered at the radio pulsar's timing position. Net counting rates for the pulsar counterparts (cf. Table 2) were obtained by subtracting an averaged background rate which we obtained from combining two different source-free regions located near to the pulsar. Power law and blackbody model spectra were then fitted to the extracted spectra by using XSPEC 12.3.1. All datasets of a pulsar counterpart were fitted simultaneously unless a temporal counting rate variability was found for e.g. binary pulsars.

Most millisecond pulsar counterparts are detected with a relatively small photon statistics, requiring to fix the hydrogen column densities in order to better constrain the remaining model parameters. If so we deduced N_H from the optical foreground reddening E(B−V) of the corresponding globular clusters (Harris 1996, updated 2003[6]). Only for PSR J1824-2452A in M28 and the two recent observations #7460 and #7461 of PSR J1740-5340 in NGC 6397 the photon statistics was sufficient to include N_H as an additional free parameter in the spectral fits.

For all 47 Tuc pulsars we grouped the extracted spectra so as to have at least 5 counts per spectral bin. 47 Tuc F+S and G+I were treated as single sources since their spectra could not be separated. The spectral parameters for most of the 47 Tuc pulsars are consistent with those reported by Bogdanov et al. (2006), except for 47 Tuc L and R. The spectral fits of these two pulsars are not well described by a single blackbody model albeit different background regions were included or N_H was let a free parameter in the fits. A composite model consisting of a blackbody plus power-law model yields a better but still not optimal description of the observed spectra.

In order to investigate whether the binary pulsars PSR J1740−5340 in NGC 6397 and J1748−2021B in NGC 6440 show spectral changes along with their variable counting rates observed at different orbital phase angles we analyzed each of their available datasets separately. As can be seen in Table 8, the photon indices obtained for a pulsar from each of the various datasets are all in agreement with each other (cf. also Huang & Becker 2010 for a more detailed discussion on PSR J1740–5340 in NGC 6397). The X-ray luminosity of PSR J1748–2021B in NGC 6440, though, changed by a factor of ~ 3 for observations taken in 2000 July and 2003 June. PSR J1748–2021B furthermore shares the non-thermal nature of its X-ray spectrum with PSR J1953+1846A in M71 (cf. Elsner et al. 2008) and PSR J1701–3006C in M62. Their photon indices are in the range $\sim 1.4 - 1.9$. For the binary pulsars PSR J1824-2452H in M28 and PSR J1748-2446 in Terzan 5 the limited photon statistics did not support to distinguish between thermal or non-thermal emission models. A blackbody and a power-law model both describe their spectra with comparable goodness (cf. Table 8). The fitted blackbody temperatures, however, are at the level of $\gtrsim 10^7\ K$, which is an order of magnitude higher than what is observed in other millisecond pulsar spectra (cf. Table 6.7 in Becker 2009). A non-thermal interpretation of their emission therefore seems more likely to us. Whether this non-thermal X-ray radiation is due to magnetospheric emission from within the pulsars' co-rotating light-cylinder or whether it arrises because of an intra-binary shock formed by the relativistic pulsar wind and the matter from the stellar companion is currently not clear.

---

[6] http://physwww.mcmaster.ca/~harris/Databases.html

For the brightest of all millisecond pulsars, PSR J1824-2452A, five observations are currently available in the Chandra data archive. Three of them were taken in 2002 and provided the basis for the results published on M28 by Becker et al. (2003). Two additional and significantly longer observations of M28 were taken in 2008, increasing the total on source exposure to 237 ksec, i.e. almost five times as much as was available in 2002. To analyze the spectrum of PSR J1824-2452A we made use of all five datasets.

The spectra based on the 2002 data were grouped so as to have at least 30 counts per spectral bin. For the 2008 data we used a grouping of 50 and 30 counts per spectral bin for the longer (#9132) and shorter (#9133) observations (cf. Table 1). It has been shown previously that the pulsar's X-radiation is dominated by non-thermal emission (Kawai & Saito 1999, Becker et al. 2003, Mineo et al. 2004). Fitting a power-law spectral model to the data yields $N_H = (0.22 \pm 0.02) \times 10^{22}\,\mathrm{cm}^{-2}$, a photon-index $\alpha = 1.13^{+0.03}_{-0.04}$, and a normalization at 1 keV of $3.43^{+0.23}_{-0.15} \times 10^{-5}$ photons $\mathrm{cm}^{-2}\ \mathrm{s}^{-1}\ \mathrm{keV}^{-1}$ ($\chi^2_\nu = 1.00$ for 168 dof). The column density is fully consistent with what is deduced from the reddening towards M28. The unabsorbed energy flux in the $0.3 - 8.0$ keV band is $f_x = 3.7^{+0.4}_{-0.3} \times 10^{-13}$ ergs $\mathrm{s}^{-1}\ \mathrm{cm}^{-2}$, yielding an X-ray luminosity of $L_x = 1.36^{+0.15}_{-0.11} \times 10^{33}$ ergs s^{-1}. If transformed to the $0.1 - 2.4$ keV ROSAT band this corresponds to $L_x = 3.76^{+0.33}_{-0.22} \times 10^{32}$ ergs s^{-1}, which is comparable with the luminosity inferred from the ROSAT data (Verbunt 2001). These luminosities imply a rotational energy $\dot{E}$ to X-ray energy conversion factor of $L_{x,0.3-8.0\,keV}/\dot{E} = 6.1 \times 10^{-4}$ and $L_{x,0.1-2.4\,keV}/\dot{E} = 2.1 \times 10^{-4}$, respectively. The phase averaged photon index obtained in our spectral fits is identical to the one deduced for PSR J1824-2452A from the observations at pulse maximum using joint ASCA and RXTE data (Kuiper et al. 2003). This is in agreement with the interpretation that its fraction of pulsed X-ray photons is 85% – 100%. Figure 16 shows the pulsar spectrum as fitted to an absorbed power-law model.

Unlike for many other millisecond pulsars (cf. Table 6.7 of Becker 2009 for a summary), modeling the X-ray spectrum of PSR J1824-2452A with a power-law does not require any additional blackbody component (e.g. associated with thermal emission from heated polar caps) to get an acceptable spectral fit. All combinations of blackbody normalizations and temperatures that were fitted along the power-law model gave reduced χ^2-values which didn't indicate a higher likelihood for such a model than the fits to a single power-law. The F-test statistic for adding the extra blackbody spectral component to the power-law model, thus, is very low.

Nevertheless, the high photon statistics provided by the archival Chandra data allows us to constrain the temperature of a presumed thermal polar cap. Defining the size of the polar cap as the foot points of the neutron star's dipolar magnetic field, the radius of the polar cap area is given by $\rho = \sqrt{2\pi R^3/cP}$ with R being the neutron star radius, c the velocity of light and P the pulsar rotation period (see e.g. Michel 1991). For PSR J1824-2452A, with a rotation period of 3.05 ms this yields a polar cap radius of $\rho \sim 2.62$ km.

As a thermal spectral component of a heated polar cap contributes mostly below ~ 1 keV, the fitted column absorption is found to be a steep function of the blackbody emitting area (corresponding to the model normalization) and temperature. To determine a polar cap temperature upper limit which is in agreement with the fitted power-law model and column absorption we fixed the absorption of the composite model as well as the power-law photon index to the upper bound set by the 1σ confidence range deduced in the power-law fit. The power-law normalization was fixed to the 1σ lower bound as this led to a higher temperature upper limit. We then computed the confidence ranges of the blackbody normalization and temperatures by leaving these parameters free. The resulting contours, computed for two parameters of interest, are shown in Figure 17.

The blackbody normalization in XSPEC is proportional to $\rho_{km}^2/d_{10\,kpc}^2$ in which ρ_{km} is the blackbody radius of the emitting area and $d_{10\,kpc}$ is the pulsar distance in units of 10 kpc. For a distance of 5.6 kpc towards M28 and a polar cap radius of 2.62 km we thus obtain a normalization of 21.88. Assuming a contribution from one polar cap only we can set a 3σ temperature upper limit of $T_{pc}^{\infty} < 1.3 \times 10^6$ K. This upper limit is at the same level as the temperatures fitted for the thermal components in the spectra of e.g. the solitary millisecond pulsar PSR J2124 – 3358 or of PSR J0437 – 4715 (cf. Table 6.7 in Becker 2009). Converting the temperature upper limit into a flux upper limit yields $f_{bb,0.3\text{–}8\,keV} \leq 1.5 \times 10^{-14}$ ergs s^{-1} cm^{-2}, corresponding to $\leq 4\%$ of the non-thermal energy flux within 0.3 – 8 keV.

The best-fit spectral models and parameters used to describe the spectra of the X-ray detected globular cluster millisecond pulsars are summarized in Table 8.

3. SUMMARY AND DISCUSSION

We have systematically studied the X-ray emission properties of 31 globular cluster millisecond pulsar counterparts in order to evaluate their spectral properties and luminosities in a consistent way. Timing analysis has been performed for all sources according to the temporal resolution available in the archival Chandra data. Making use of unpublished data on M28, M4 and NGC 6752 allowed us to obtain further constraints for the millisecond pulsar counterparts located in these clusters. Counting rate and energy flux upper limits were computed for 36 globular cluster millisecond pulsars for which no X-ray counterparts could be detected.

By spring 2010 emission from 98 rotation-powered pulsars has been detected in the soft X-ray band. 51 of these sources belong to the group of galactic field pulsars whereas the other 47 sources are recycled pulsars. 31 of them are located in nine globular clusters. Coherent X-ray pulses are detected from 10 millisecond pulsars of which four are in a globular cluster. These are PSR J0024-7204 D,O,R in 47 Tuc for which we measured a pulsed fraction of $\sim 60\%$ and PSR J1824-2452A in M28 which has $\sim 85\%$ of its X-rays pulsed. Their X-ray pulse profiles are all characterized by two peaks, which in the case of PSR J1824-2452A are narrow (phase width $\sim 10^{o}$ and $\sim 20^{o}$ (FWHM) for the first and second peak) and broader (typical phase width $\sim 100^{o}$ and $\sim 150^{o}$ (FWHM)) in the case of J0024-7204 D,O,R.

Comparing the X-ray lightcurves with the corresponding radio profiles shows that there is some correspondence between both. For PSR J1824-2452A the main X-ray pulse component appears to be almost phase aligned with the main radio pulse. No correspondence of the remaining two peaks seen at 800 MHz is found in the X-ray profile. The 47 Tuc pulsars J0024-7204 D,O have two radio peaks observed at 1400 MHz (Freire et al., 2010, in prep.), albeit their second radio peak has a much lower intensity than the main peak. PSR J0024-7204D shows an asymmetry in the main radio peak as the X-ray peaks do. The profile of PSR J0024-7204 R is characterized by a narrow X-ray peak followed by a broader pulse component covering the remaining rotation phase. The profile at 1400 MHz shows a striking gross similarity, consisting of a narrow main pulse and a broader pulse component which by itself has a sub-structure (Freire et al., 2010, in prep.). Clearly, a better photon statistics is required in order to establish this correspondence.

36 of the 67 millisecond pulsars which we have considered in this work are in binaries. X-ray flux variability either on time scales comparable with the pulsar's orbit period or even longer was found for only three of them; the binary pulsars PSR J0024-7204W in 47 Tuc, PSR J1748-2021B in NGC 6440 and PSR J1740-5340 in NGC 6397. Some low-significant evidence for a flux variability along their binary motion was found for PSR J1824-2452H and J1824-2452G.

Spectral information is available from all 31 globular cluster millisecond pulsar counterparts (cf. Table 8). The complexity of the spectral models which could be tested and the accuracy of the fitted spectral parameters, however, are strongly inhomogeneous among all of them. This is not only because of a diversity of the column absorption towards the various clusters but also because of varying photon statistics, which for fainter sources often do not even allow to distinguish between simple blackbody and power-law spectral models.

PSR J1824-2452A is the brightest among all millisecond pulsars and is a non-thermal Crab-like X-ray emitter. Using the 2002 Chandra data, Becker et al. (2003) found in its X-ray spectrum some evidence for a possible line feature at $\sim 3.3\,\mathrm{keV}$ (cf. Figure 2 in Becker et al. 2003). The new data taken in 2008 supersede the previous data in photon statistics and sensitivity and do not confirm the presence of this feature. A 3σ temperature upper limit of 1.3×10^6 K is deduced for a presumed thermal polar cap contribution. This is at the same level as observed in spectral fits of other millisecond pulsars. That non-thermal radiation is the dominating emission component in PSR J1824-2452A thus does not exclude the existence of a thermal polar cap of similar properties than observed in e.g. PSR J0437-4715 or PSR J2124-3358 (cf. Table 6.7 in Becker 2009). The 47 Tuc pulsars all fit relatively well with a thermal spectrum or a composite spectral model consisting of a blackbody and power-law. The latter model especially fits the spectra of e.g. PSR J0024-7204 O,R for which X-ray pulses are detected.

Grindlay et al. (2001) suggested that the X-ray efficiency for the 47 Tuc millisecond pulsars is $L_\mathrm{X} \propto \dot{E}^{0.48\pm0.15}$. Such dependence is obviously less steep than the linear relation $L_\mathrm{X} \sim 10^{-3}\dot{E}$ found for the isotropic X-ray luminosity of rotation-powered pulsars by Becker & Trümper (1997). Bogdanov et al. (2006) found a relation of $L_\mathrm{X} \propto \dot{E}^{0.2\pm1.1}$ for the 47 Tuc pulsars using more significant Chandra data taken in September/October 2002. We have reexamined the isotropic X-ray conversion efficiency of the globular cluster pulsar population in adding the results reported in this paper into the data pool. To compute the spin-down power $\dot{E}$ of the globular cluster pulsars we used the estimated intrinsic spin-down rate $\dot{P}$ reported in the literature. Pulsars which turned out to be variable were excluded from the correlation. As both, emission from heated polar caps and non-thermal emission finally appears to be powered by the rotation of the star the X-ray luminosities from both spectral components were added and correlated with $\dot{E}$. Adopting the absorption-corrected isotropic X-ray luminosity listed in Table 8 and its statistical 1-σ error we fitted $\log L_X = (14.49 \pm 4.47) + (0.48 \pm 0.11)\log\dot{E}$ with a correlation coefficient 0.68.

Correlating the spin-down energy and isotropic X-ray luminosity of ~ 80 rotation-powered pulsars for which spectral information was obtained in Chandra and/or XMM-Newton observations Becker (2009) fitted

$$L_X(0.1-2\,\mathrm{keV}) = 10^{-3.24^{+0.26}_{-0.66}}\,\dot{E}^{0.997^{+0.008}_{-0.001}}$$

in which the errors in L_x have been fully taken into account and were used to weight the data points. Although the data includes three times as much pulsars than were available with ROSAT the correlation is still in good agreement with $L_\mathrm{X}(0.1-2.4\,\mathrm{keV}) \sim 10^{-3}\,\dot{E}$ (cf. Figure 18). With the larger database it now becomes evident that this relation represents an averaged approximation to the X-ray efficiency rather than a fixed correlation. This was already suggested by Becker & Trümper (1997) and may be due to the fact that ROSAT with its limited sensitivity was able to detect essentially only the brightest pulsars. With the higher sensitivity of XMM-Newton and Chandra more faint pulsars could be detected in which e.g. the orientation of their magnetic/rotational axes to the observers line of sight might not have been optimal. As no beaming correction can be applied to the observed luminosities the X-ray efficiency of those pulsars appears to be smaller, even though their spin-down energy might be comparable to more efficient emitters.

As far as the X-ray efficiency from the globular cluster millisecond pulsars is concerned it can be seen from Figure 19 that their X-ray luminosities are well within the scatter of other data points at this spin-down energy level. Within the uncertainties of the deduced X-ray luminosities it is therefore not justified to conclude that these pulsars have an X-ray efficiency which is different from the one observed for e.g. field millisecond pulsars. Millisecond pulsars in the galactic plane and in globular clusters thus appear to show no distinct differences in their X-ray emission properties.

REFERENCES

Abdo, A.A., Ackermann, M., Atwood, W.B., et al., 2009a, ApJ, 699, 1171

Abdo, A.A., Ackermann, M., Ajello, M., et al., 2009b, Science, 325, 848

Backer D.C., Sallmen S., 1997, ApJ, 114, 1539

Becker, W., 2009, in Astrophysics and Space Science Library, Vol. 357, ed. W. Becker, 91–140

Becker, W., Swartz, D.A., Pavlov, G., et al. 2003, ApJ, 594, 798

Becker, W., Trümper, J., 1999, A&A, 341, 803

Becker, W., Trümper, J., 1997, A&A, 326, 682

Bégin, S. 2006, Thesis, University of British Columbia

Bogdanov, S., Grindlay, J.E., Heinke, C.O., et al., 2006, ApJ, 646, 1104

Bogdanov, S., Grindlay, J.E., Heinke, C.O., et al., 2005, ApJ, 630, 1029

Buccheri R., De Jager O.C., in Timing Neutron Stars, eds H.Ögelman, E.P.J. van den Heuvel, p95, Kluwer Academic Publishers, 1989

Camilo, F.; Rasio, F. A., 2005, ASPC, 328, 147

Camilo, F., Lorimer, D.R., Freire, P., Lyne, A.G., Manchester, R.N., 2000, ApJ, 535, 975

Cocozza, G., Ferraro, F.R., Possenti, A., et al., 2008, ApJ, 679, L108

Cameron, P.B., Rutledge, R.E., Camilo, F., et al., 2007, ApJ, 660, 587

D'Amico, N., Possenti, A., Fici,I., et al., 2002, ApJ, 570, L89

D'Amico, N., Possenti, A., Manchester, R.N., et al., 2001, ApJ, 561, L89

Danner, R., Kulkarni, S.R., Saito, Y., Kawai, N., 1997, Nat, 388, 751

De Jager O.C., 1987, thesis, Potchefstromm University for Christian Higher Education, South Africa

Elsner, R.F., Heinke, C.O., Cohn, H.N., et al., 2008, ApJ, 687, 1019

Freire, P.C., Ransom, S.M., Bégin, S., et al., 2008, ApJ, 675, 670

Freire, P.C., Camilo, F., Kramer, M., Lorimer, D.R., Lyne, A.G., Manchester, R.N., D'Amico, N., 2003, MNRAS, 340, 1359

Fregeau, J.M., 2008, ApJ, 673, L25

Grindlay, J.E., Bogdanov, S., 2009, in Astrophysics and Space Science Library, Vol. 357, ed. W. Becker, 165–180

Grindlay, J.E., Heinke, C.O., Edmonds, P.D., et al., 2001, ApJ, 563, 53

Huang, R.H.H., Becker, W., 2010, A&A, 510, 67

Ivanova, N., Heinke, C.O., Rasio, F. A., Belczynski, K., & Fregeau, J. 2008, MNRAS, 386, 553

Kawai N., Saito Y., 1999, Proc. 3rd INTEGRAL Workshop, Taormina, Astroph. Lett. & Comm. 38, 1

Kuiper, L., Hermsen, W., Stappers, B., 2003, in *Pulsars, AXPs and SGRs observed with BeppoSAX and Other Observatories*, eds G. Cusumano, E. Massaro & T. Mineo, 2003, p31

Lyne, A.G., Brinklow, A., Middleditch, J., Kulkarni, S.R., Backer, D.C., 1987, Nature, 328, 399

Manchester, R.N., Hobbs, G.B., Teoh, A., Hobbs, M., 2005, AJ, 129, 1993

Mineo, T., Cusumano, G., Massaro, E., Becker, W., Nicastro, L., 2004, A&A, 423, 1045

Ransom, Scott M., 2008, in 40 YEARS OF PULSARS: Millisecond Pulsars, Magnetars and More, AIP Conference Proceedings, Vol. 983, 415

Ransom, S.M., Stairs, I.H., Backer, D.C., et al., 2004, ApJ, 604, 328

Rasio, F.A., Pfahl, E.D., Rappaport, S., 2000, ApJ, 532, 47

Rots, A., 2006, Bulletin of the American Astronomical Society, 38, 1131

Rutledge, R.E., Fox, D.W., Kulkarni, S.R., et al., 2004, ApJ, 613, 522

Saito, Y., Kawai, N., Kamae, T., Shibata, S., Dotani, T., Kulkarni, S.R., 1997, ApJ, 477, L37

Swanepoel J.W.H., de Beer C.F., Loots H., 1996, ApJ, 467, 261

Verbunt, F., 2001, A&A, 368, 137

Webb, N.A., Knödlseder, J., 2010, Proceedings of the 2009 Fermi Symposium, arXiv:1001.1855v1

Zavlin, V.E., 2007, Ap&SS ,308, 297

Acknowledgments

We thank J. Trümper for his comments and P. Freire for making the radio profiles of PSR J0024–7204D, J0024–7204O and J0024–7204R available to us prior publication. H.H. Huang acknowledges support by the International Max-Planck Research School on Astrophysics, IMPRS. We acknowledge the use of the Chandra data archive.

This preprint was prepared with the AAS LaTeX macros v5.0.

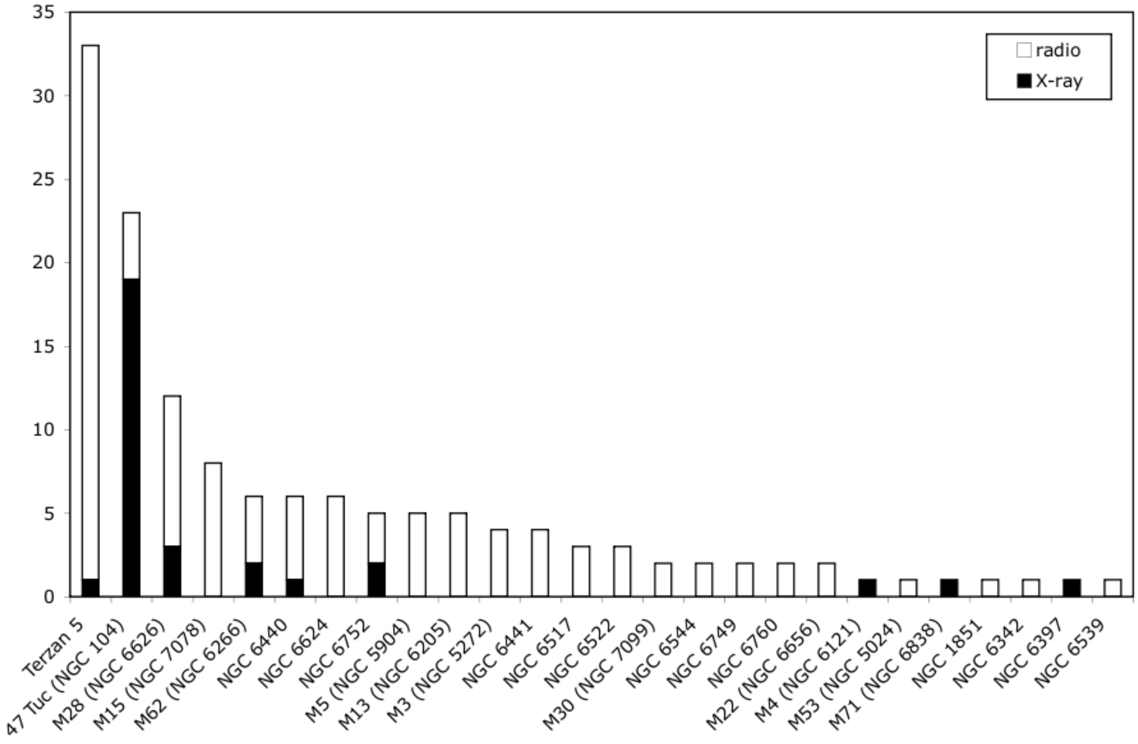

Fig. 1.— A histogram of radio and X-ray detected millisecond pulsars in globular clusters. (Status: spring 2010).

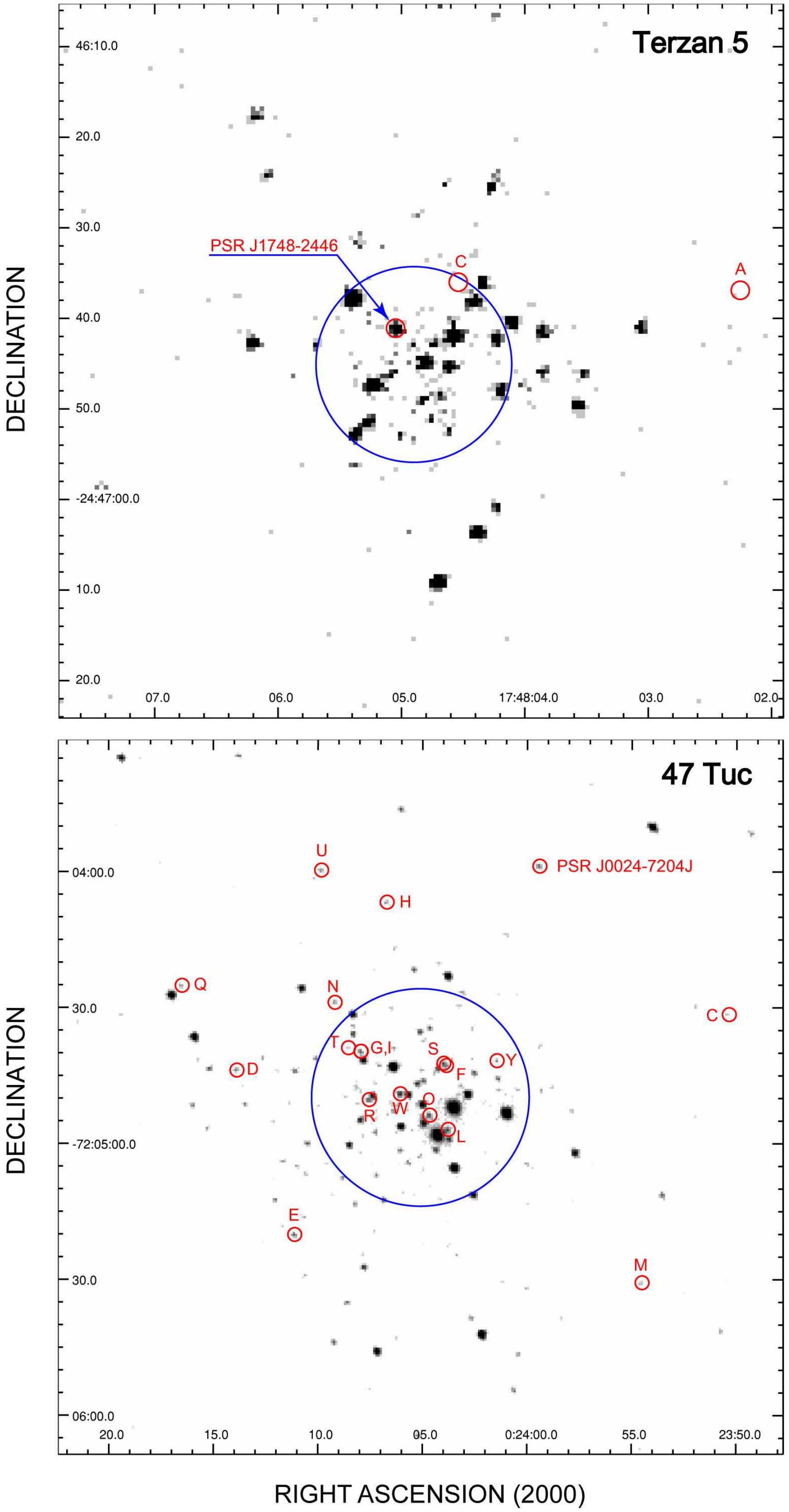

Fig. 2.— Chandra ACIS-S view on the globular clusters Terzan 5 and 47 Tuc. The clusters core radius and the position of known millisecond pulsars are indicated by blue and red circles, respectively. (Status: spring 2010).

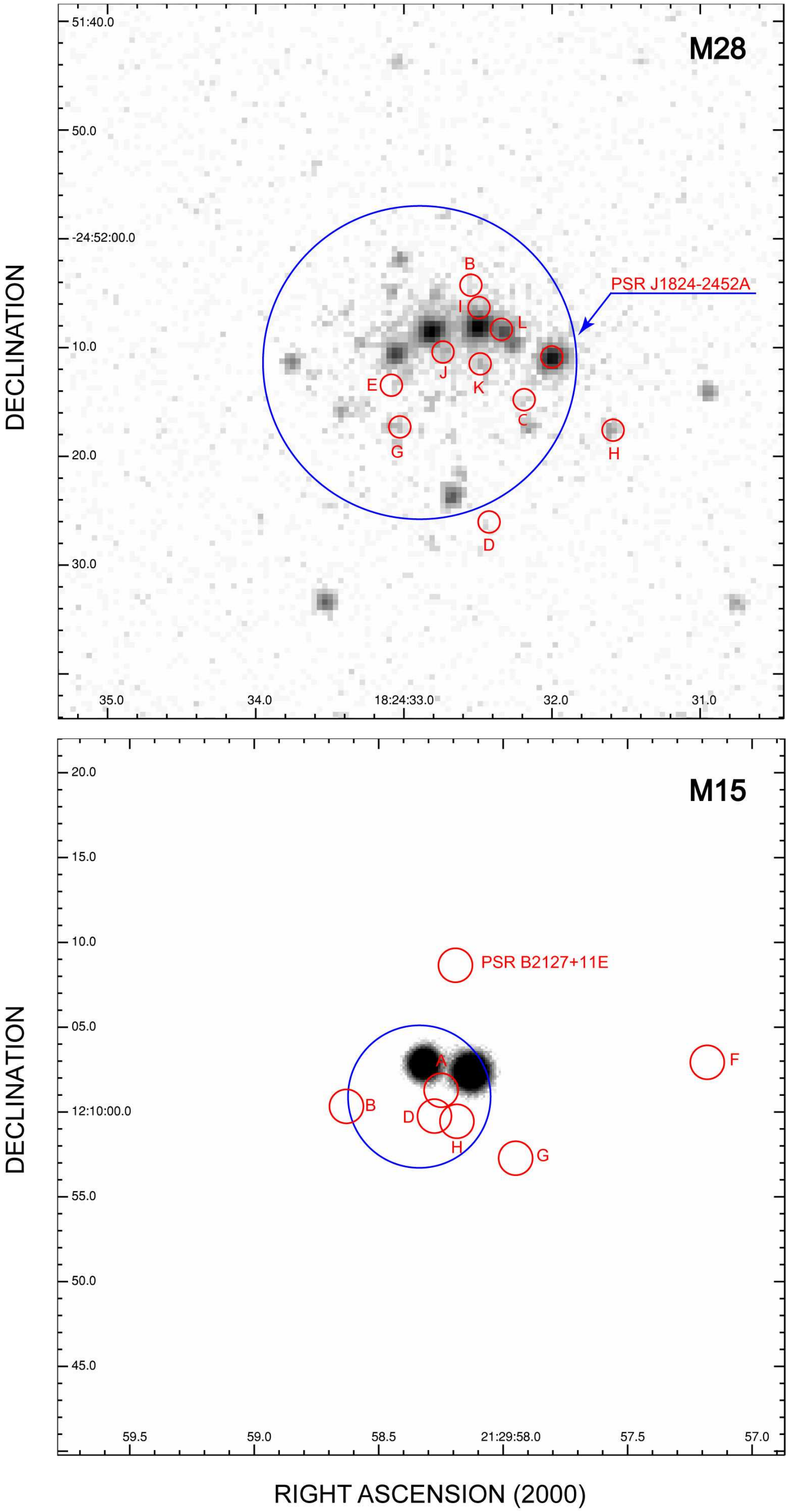

Fig. 3.— Chandra ACIS-S view on the globular clusters M28 (NGC 6626) and the HRC-I view on M15 (NGC 7078). The clusters core radius and the position of known millisecond pulsars are indicated by blue and red circles, respectively. (Status: spring 2010).

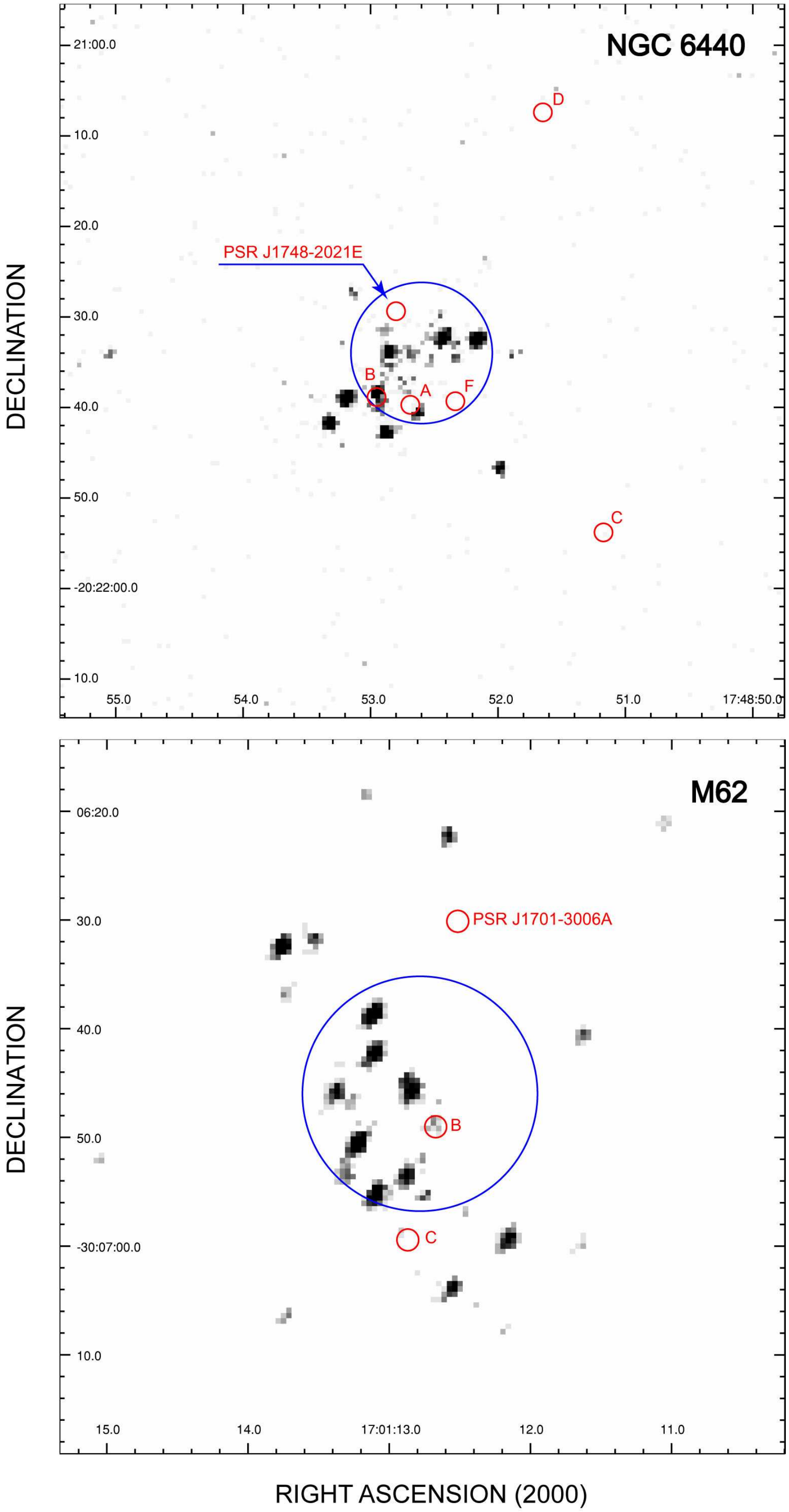

Fig. 4.— Chandra ACIS-S view on the globular clusters NGC 6440 and M62 (NGC 6266). The clusters core radius and the position of known millisecond pulsars are indicated by blue and red circles, respectively. (Status: spring 2010).

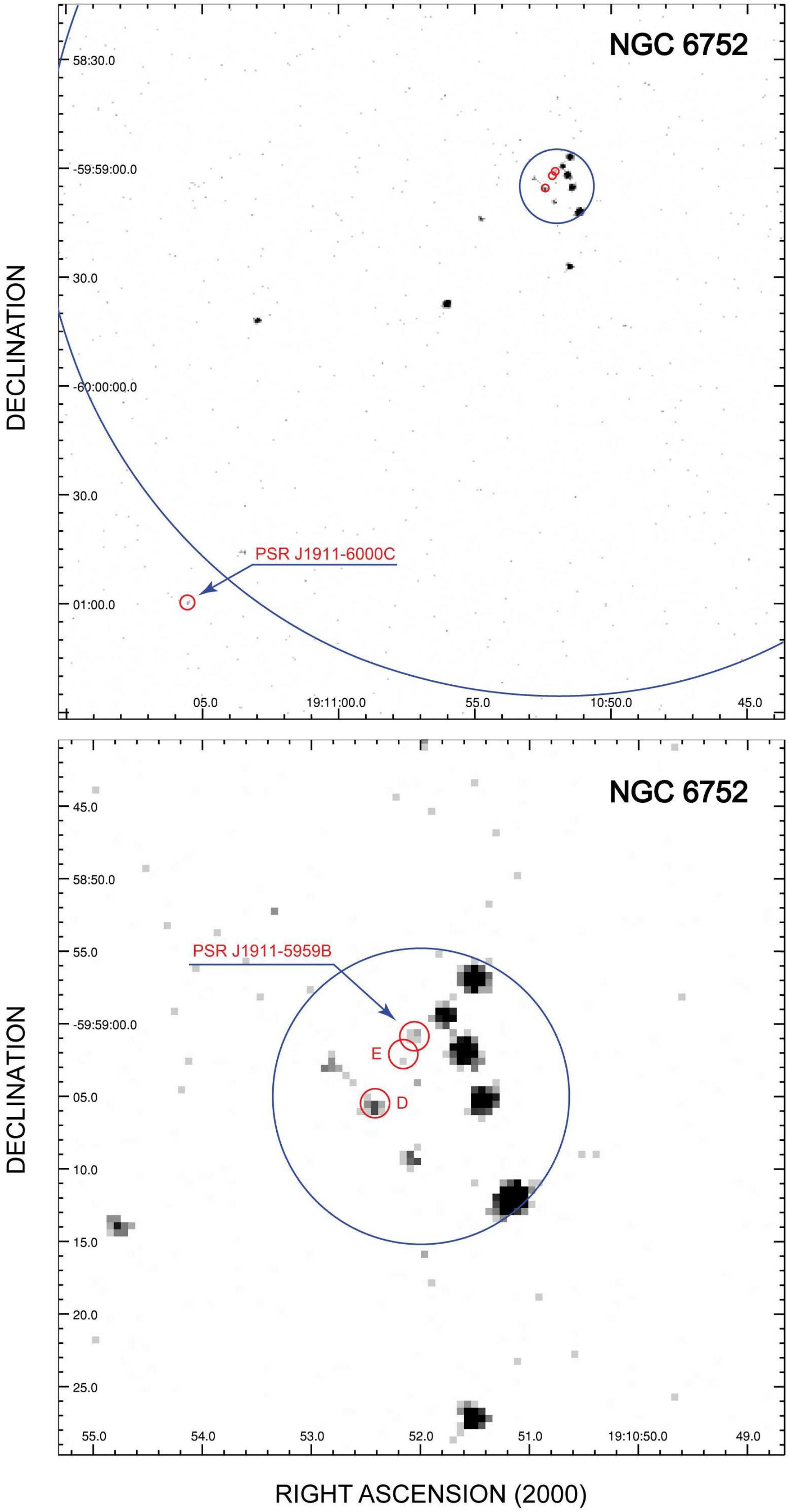

Fig. 5.— Chandra ACIS-S view on the globular clusters NGC 6752. The clusters core and half-mass radius (inner/outer circles) and the position of known millisecond pulsars are indicated by blue and red circles, respectively. The bottom figure shows a zoom in of the top figure. (Status:

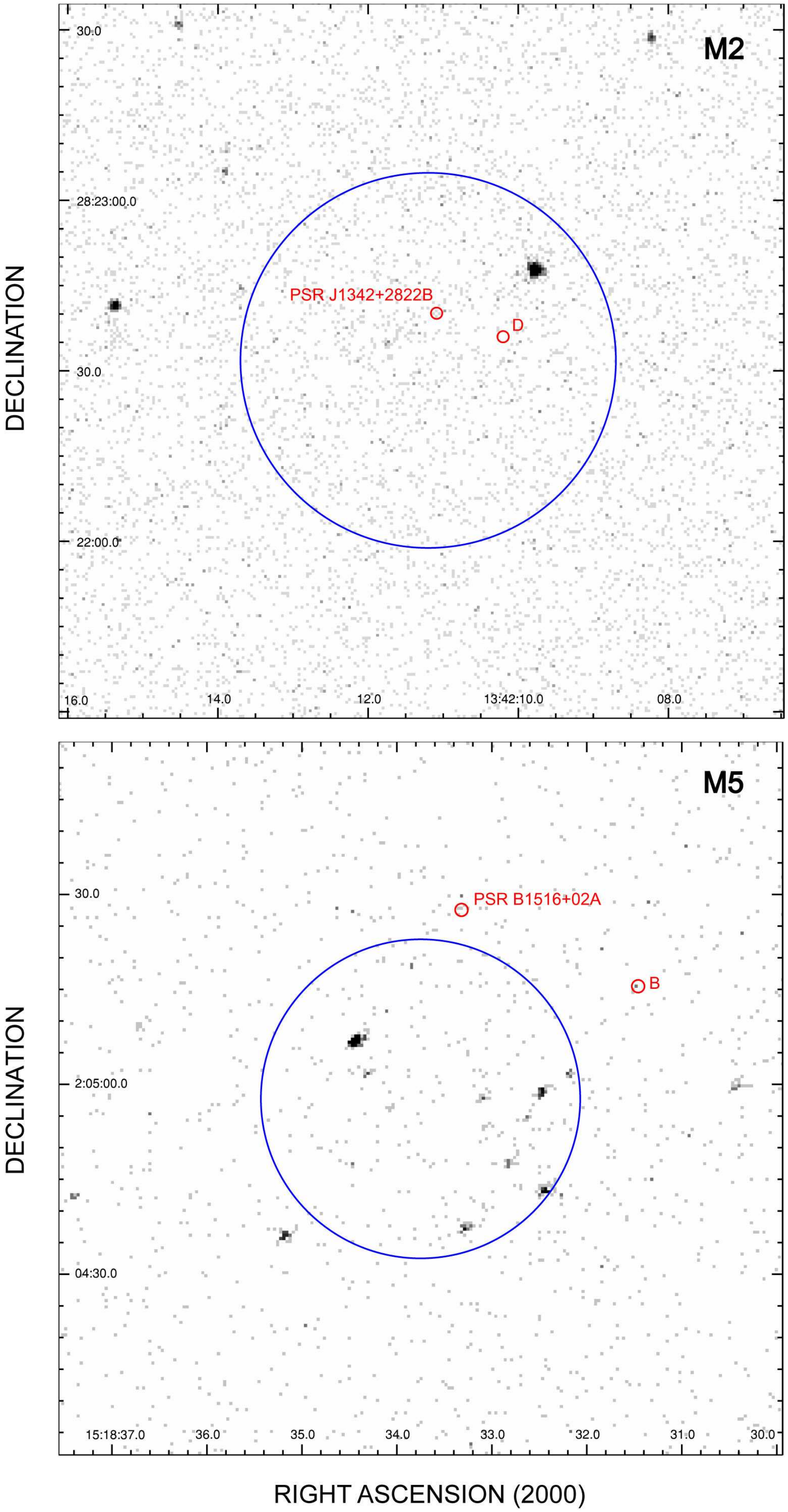

Fig. 6.— Chandra ACIS-S view on the globular clusters M3 (NGC 5272) and M5 (NGC 5904). The clusters core radius and the position of known millisecond pulsars are indicated by blue and red circles, respectively. (Status: spring 2010).

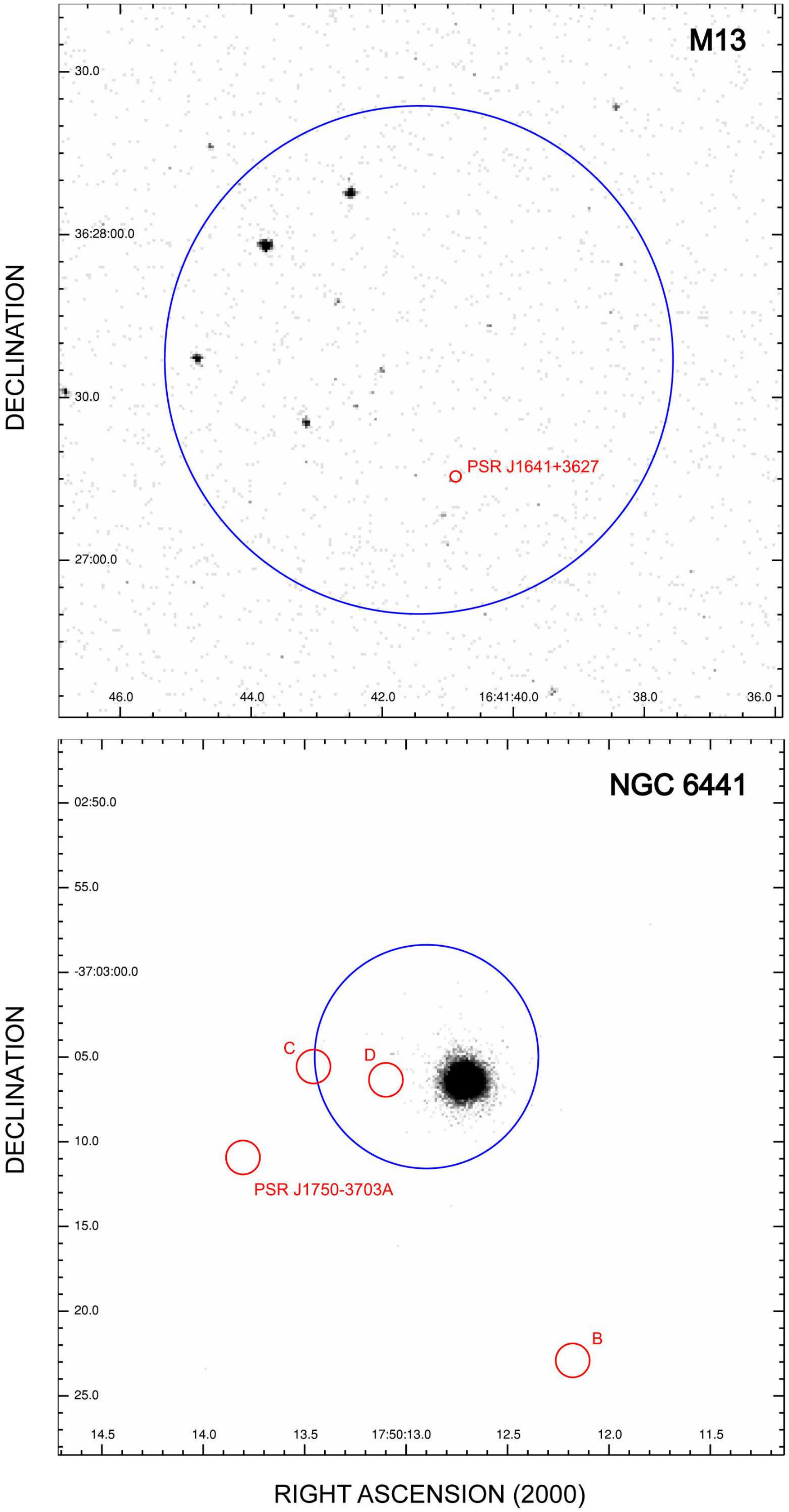

Fig. 7.— Chandra ACIS-S view on the globular clusters M13 (NGC 6205) and the HRC-I view on NGC 6441. The clusters core radius and the position of known millisecond pulsars are indicated by blue and red circles, respectively. (Status: spring 2010).

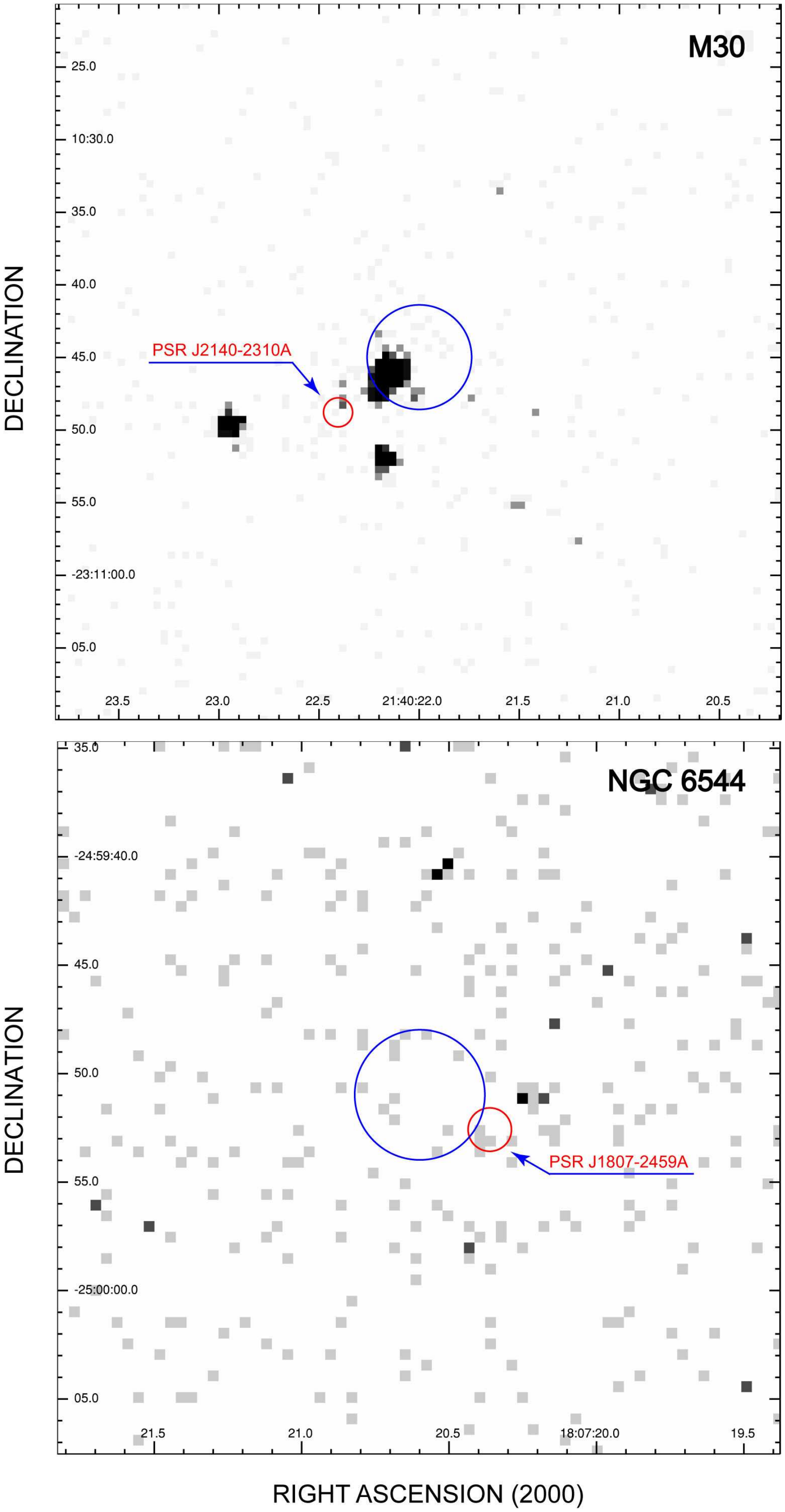

Fig. 8.— Chandra ACIS-S view on the globular clusters M30 (NGC 7099) and NGC 6544. The clusters core radius and the position of known millisecond pulsars are indicated by blue and red circles, respectively. (Status: spring 2010).

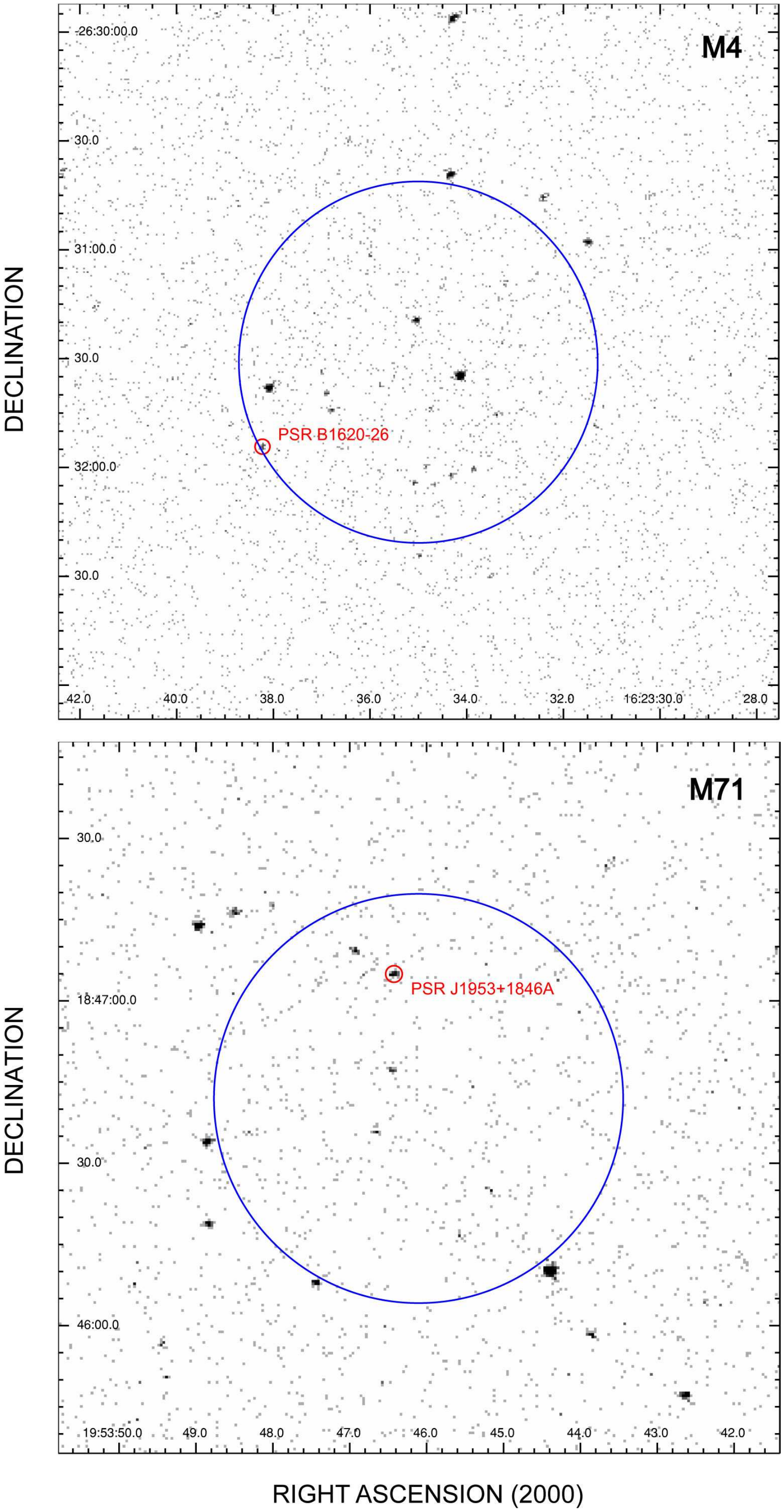

Fig. 9.— Chandra ACIS-S view on the globular clusters M4 (NGC 6121) and M71 (NGC 6838). The clusters core radius and the position of known millisecond pulsars are indicated by blue and red circles, respectively. (Status: spring 2010).

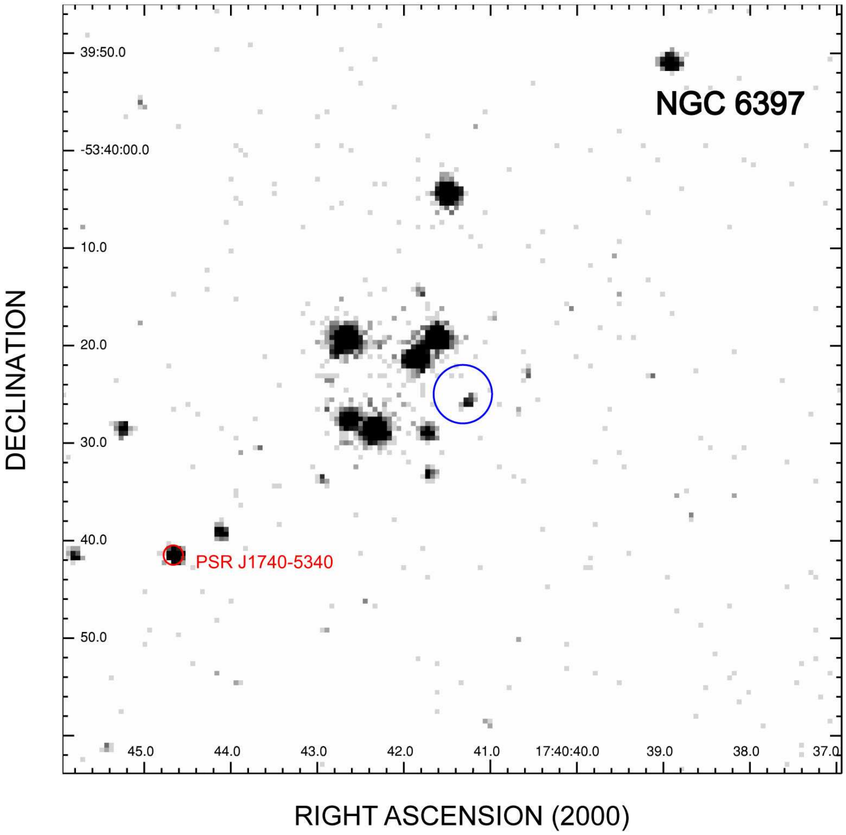

Fig. 10.— Chandra ACIS-S view on the globular clusters NGC 6397. The clusters core radius and the position of known millisecond pulsars are indicated by blue and red circles, respectively. (Status: spring 2010).

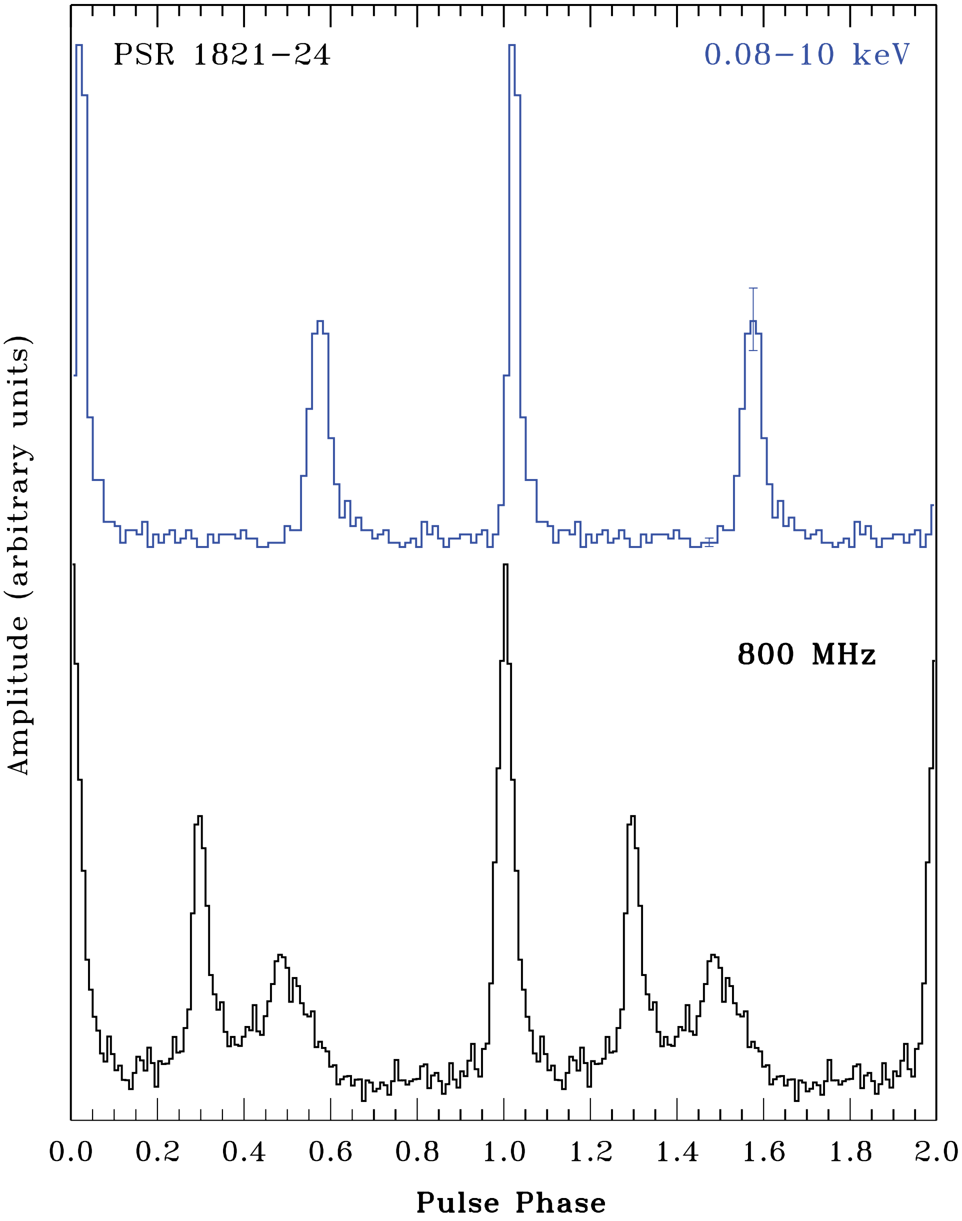

Fig. 11.— Integrated pulse profiles of the globular cluster pulsar PSR J1824–2452A as observed with the Chandra HRC-S (*top*) and with the NRAO at 800 MHz (*bottom*) by Backer & Sallmen (1997). Two phase cycles are shown for clarity. The X-ray pulse profiles are characterized by two narrow peaks with a phase separation of $\sim 0.449 \pm 0.0009$ between the two peaks. The radio profile at 800 MHz depicts three pulse components, with the main radio peak leading the second and third. The dominating radio pulse is leading the main X-ray pulse by 0.0243 in phase. The uncertainty of the ralative phase is ± 1 bin ($\sim 38\mu$s) in the X-ray profile. Phase zero corresponds to JD(TDB@SSB)=2451468.5009909072.

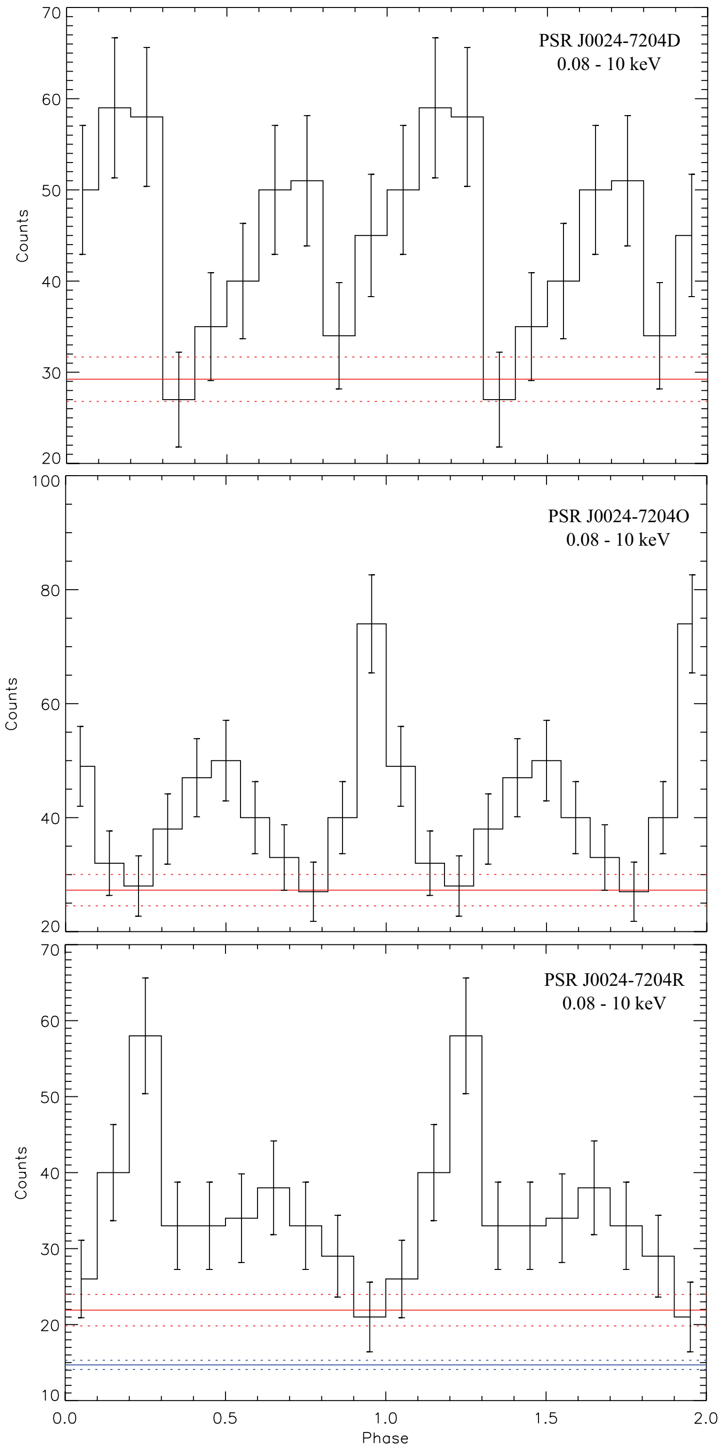

Fig. 12.— Integrated pulse profiles of the 47Tuc pulsars PSR J0024–7204 D,O,R. Two phase cycles are shown for clarity. The profiles are characterized by two pulse peaks per rotation period. The red solid and dotted lines indicate the DC level and its 1σ uncertainty. The blue solid and dotted lines in J0024–7204R indicate the level of background contribution which is 14.7 ± 1.2 cts/bin. For J0024–7204D and J0024–7204O it is 18.6 ± 1 and 17 ± 1.2 cts/bin, respectively. Phase zero corresponds to JD(TDB@SSB)=2451600.5, 2453733.50981, and 2453734.15963 in the plots of PSR J0024–7204 D,O,R.

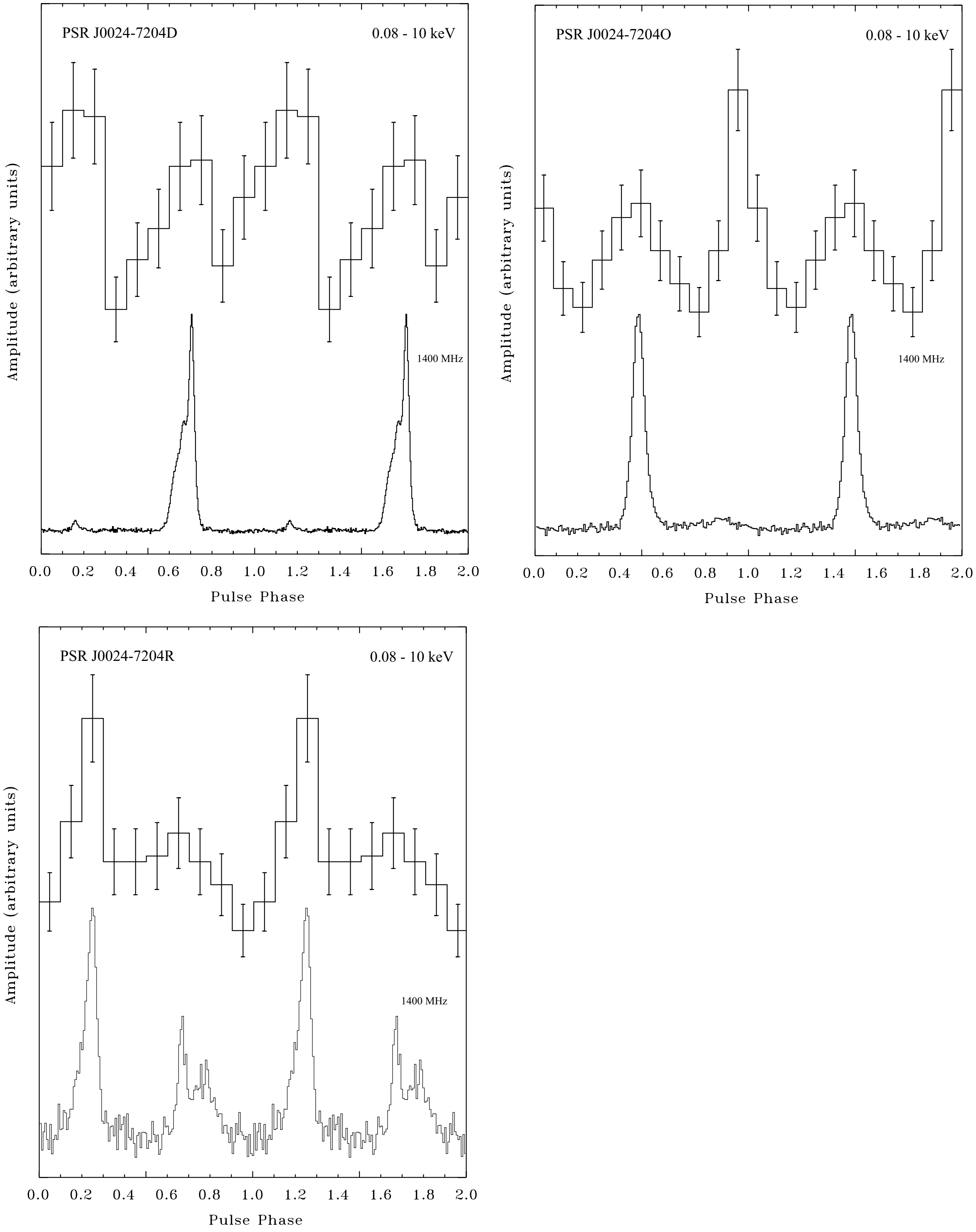

Fig. 13.— Integrated X-ray and radio pulse profiles of the 47Tuc pulsars PSR J0024–7204 D,O,R. Two phase cycles are shown for clarity. The relative phase allignement is arbitrary. The X-ray and radio profiles of J0024–7204R show an interesting gross similarity. (Radio profiles from Freire et al. 2010, im prep.)

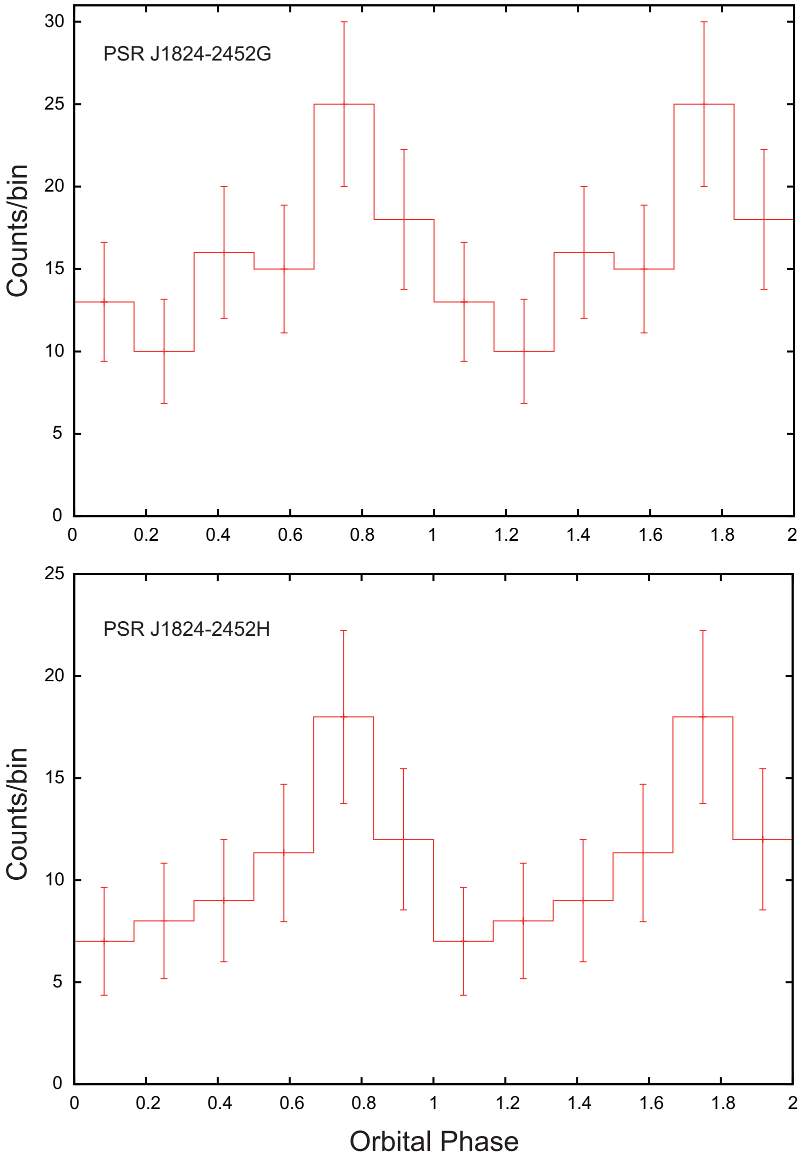

Fig. 14.— Lightcurves of the pulsars PSR J1824-2452G (top) and J1824-2452H (bottom) in M28. The data were binned into six phase bins. Error bars indicate the 1σ uncertainty. Two phase cycles are shown for clarity.

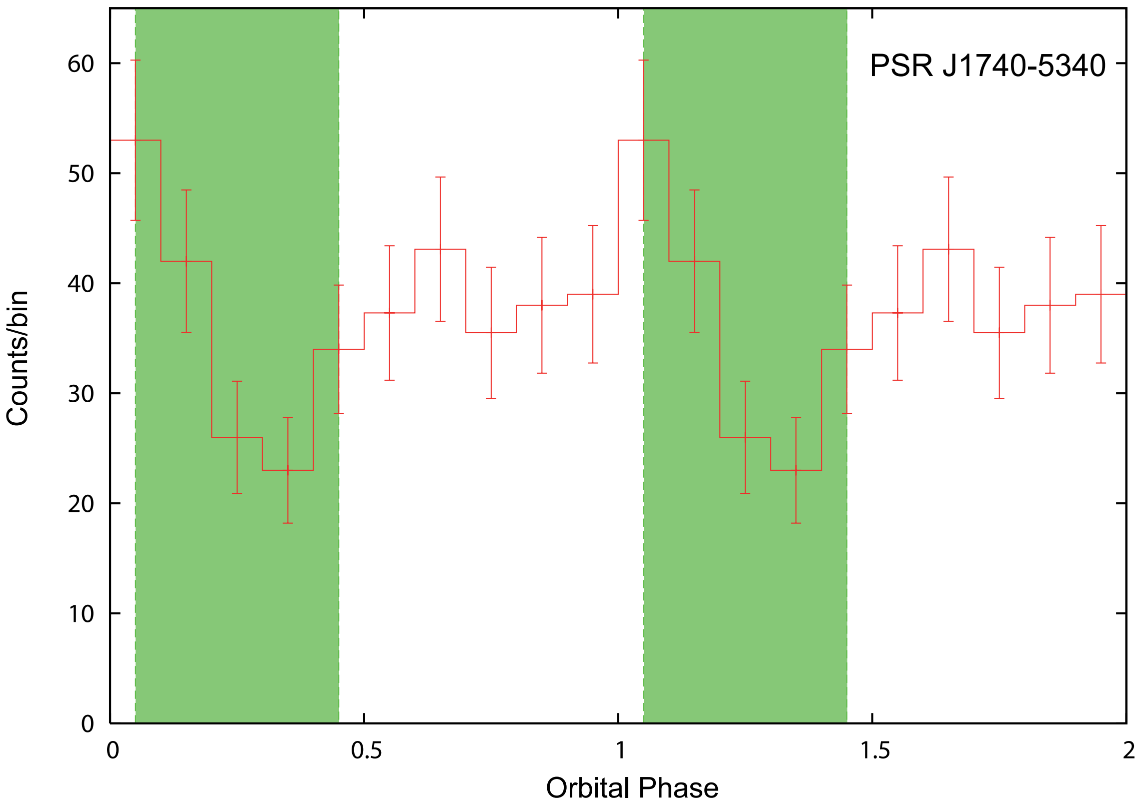

Fig. 15.— Lightcurve of PSR J1740 – 5340. Two phase cycles are shown for clarity. The background noise level is found to be at ~ 0.35 counts/bin. $\phi = 0.0$ corresponds to the ascending node of the pulsar orbit. Error bars indicate the 1σ uncertainty. The shaded phase regions mark the phases were the radio pulses eclipse.

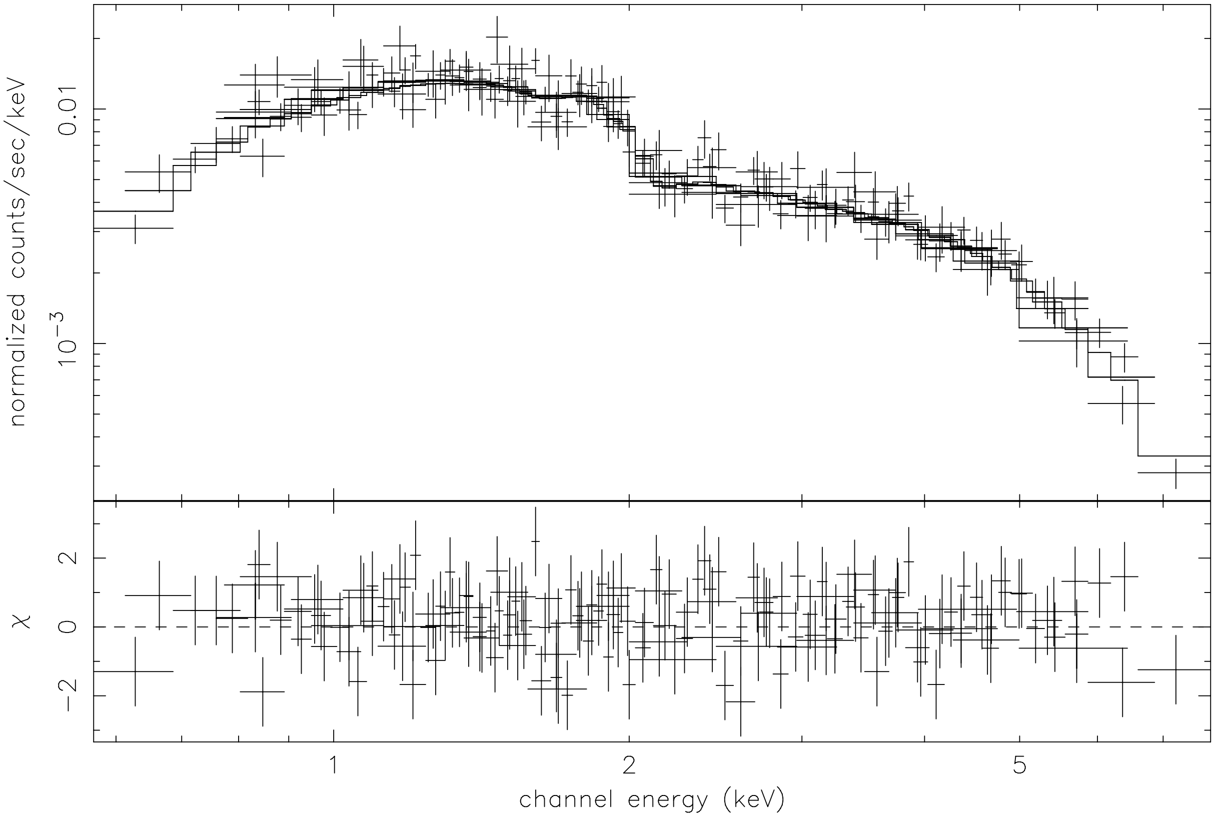

Fig. 16.— Energy spectrum of the millisecond pulsar PSR J1824-2452A in M28 obtained from the Chandra observations taken in 2002 and 2008 and fit to an absorbed power-law model (*upper panel*) and contribution to the χ^2 fit statistic (*lower panel*).

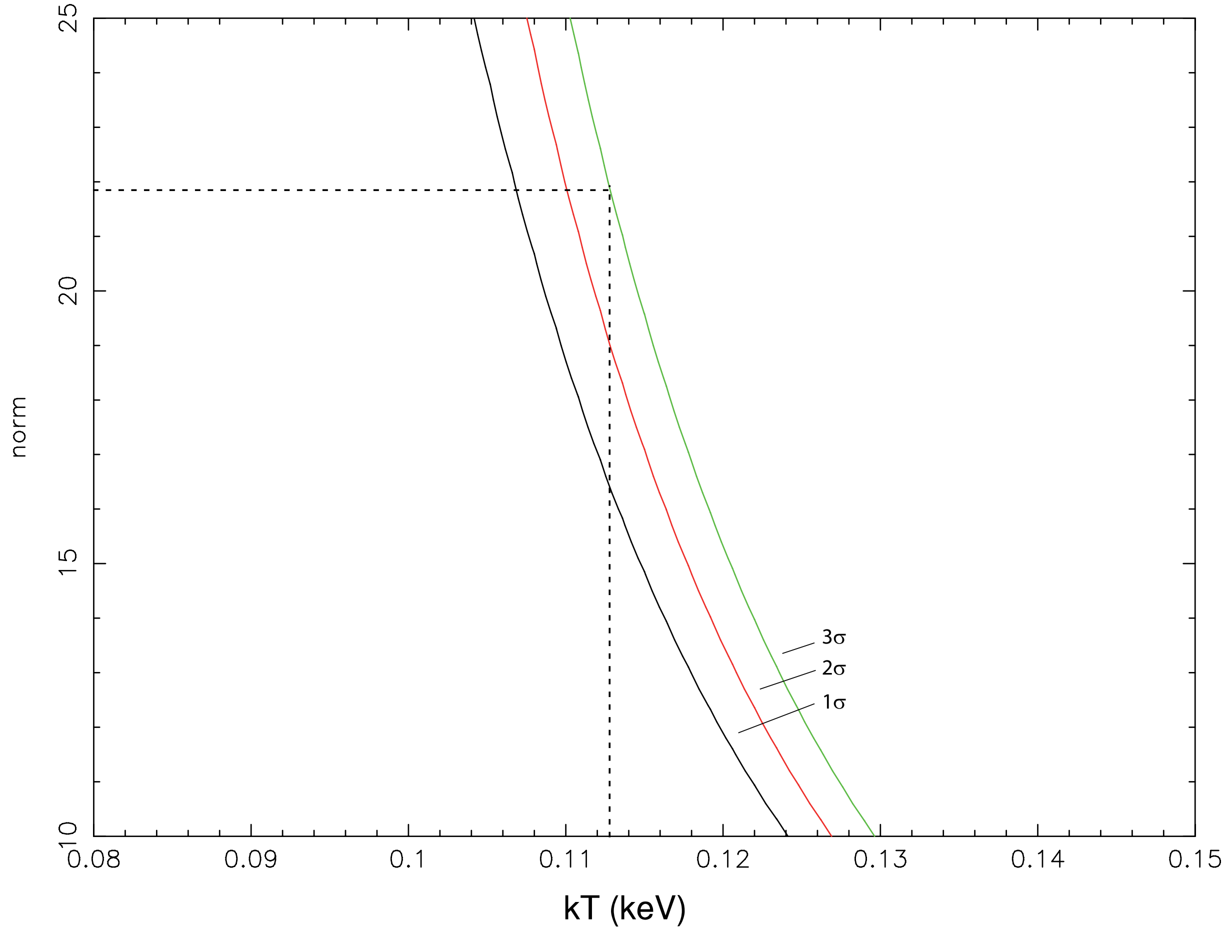

Fig. 17.— Portion of the confidence contours showing the blackbody normalization versus blackbody temperature for the composite model (see text). The horizontal line at a normalization of 21.88 corresponds to a polar cap radius of 2.62 km and a pulsar distance of 5.6 kpc. The contours correspond to χ^2_{min} = 167.5 plus 2.3, 6.17 and 11.8 which are the 1σ, 2σ and 3σ confidence contours for 2 parameters of interest.

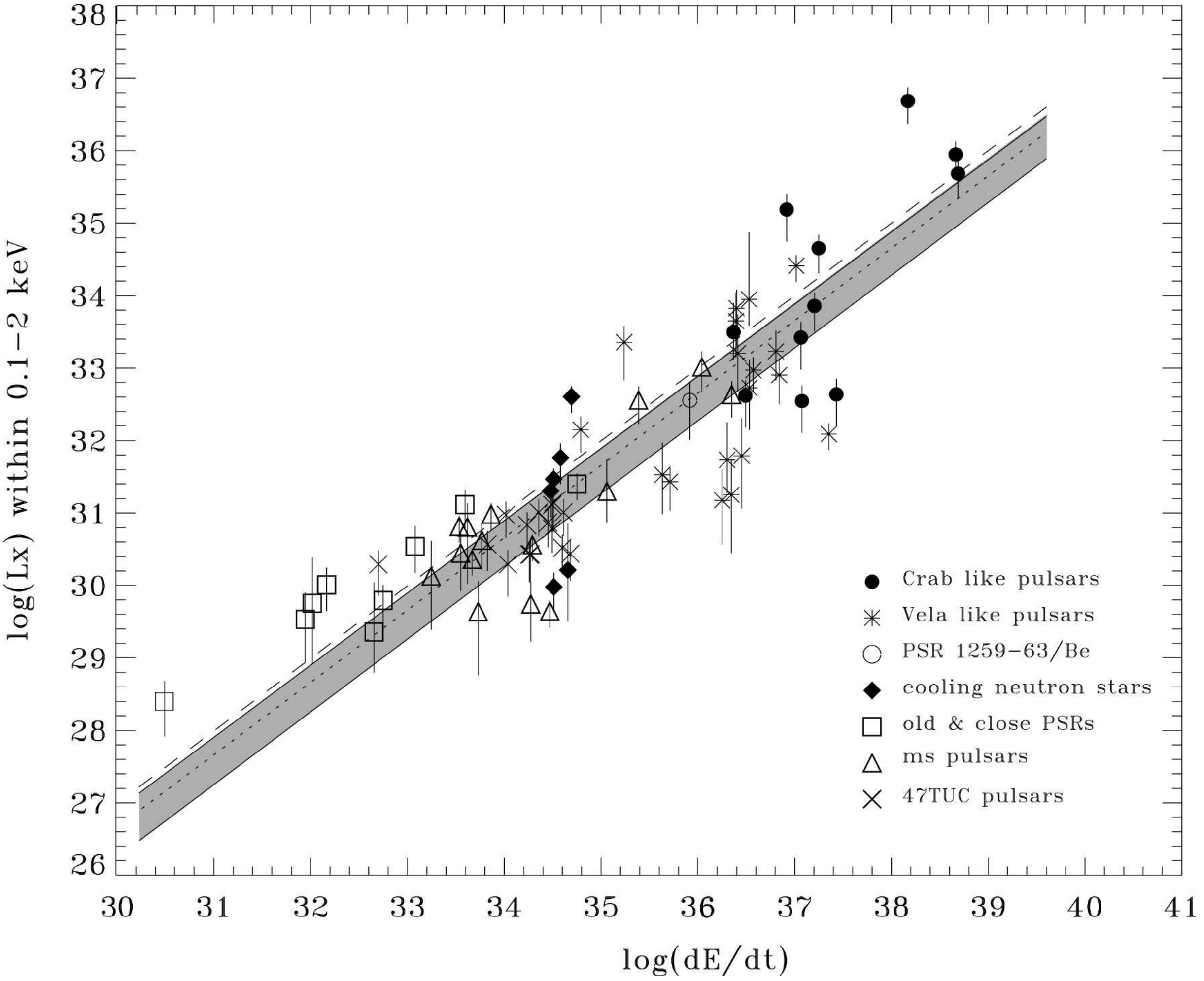

Fig. 18.— Isotropic X-ray luminosity vs. spin-down energy of X-ray detected rotation-powered pulsars. (Status: spring 2010)

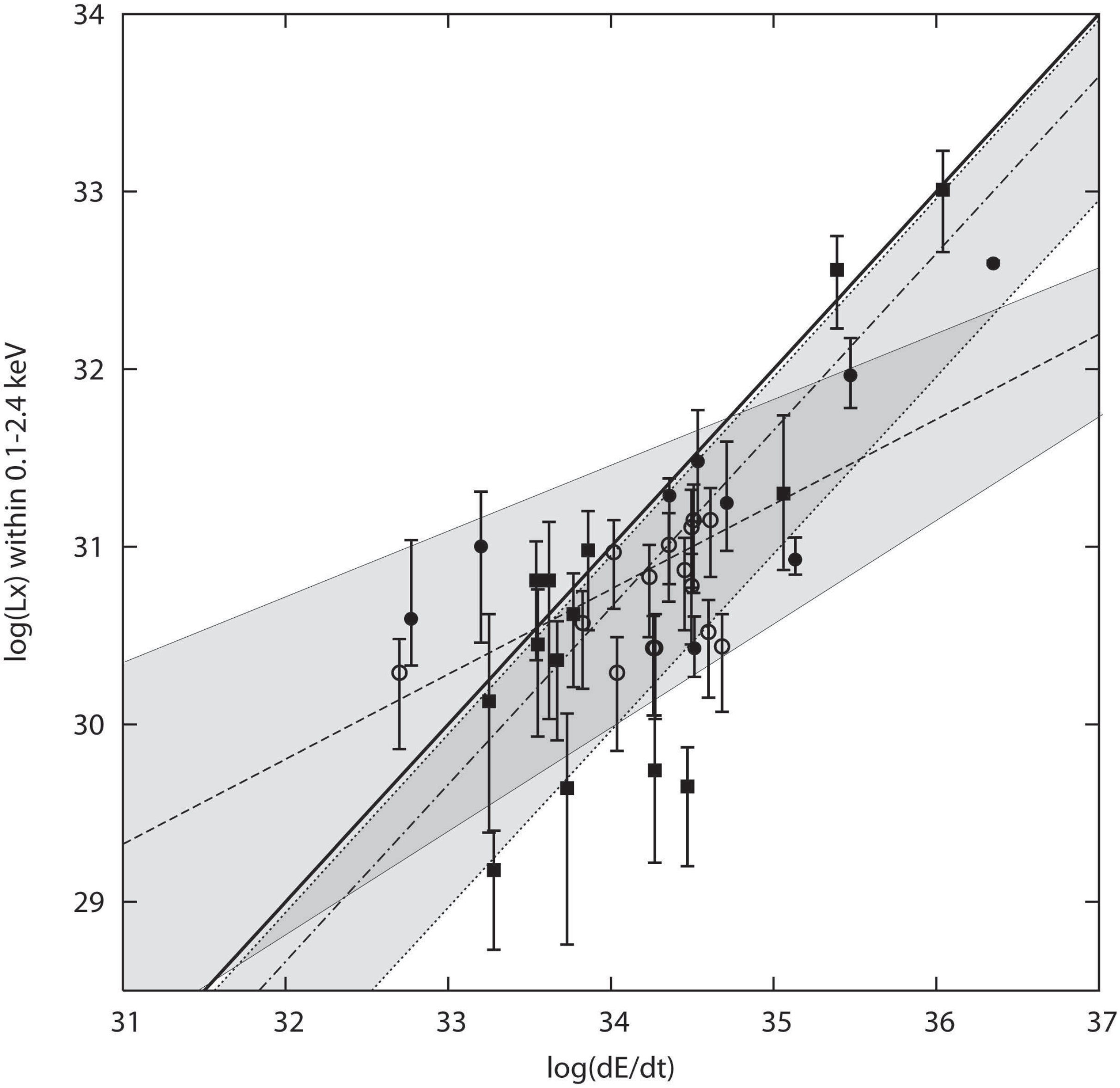

Fig. 19.— Isotropic X-ray luminosity vs. spin-down energy of X-ray detected millisecond pulsars. Galactic field millisecond pulsars are represented by *filled squares*, 47 Tuc pulsars by *open circles* and other globular cluster pulsars by *filled circles*. The solid line represents $L_{\mathrm{X},0.1\text{–}2.4\,\mathrm{keV}} = 10^{-3}\dot{E}$ (Becker & Trümper 1997) while the dot-dashed and dotted lines with its gray-shaded 1σ uncertainty range is from a fit to all X-ray detected millisecond pulsars (Becker 2009; cf. Figure 15). The dashed line and its gray-shaded 1σ uncertainty range is from correlating the spin-down energy and the X-ray luminosities of the globular cluster millisecond pulsars only.

Table 1. Chandra observations of globular clusters which are known to host millisecond pulsars. The table is ordered top-down according to the number of radio millisecond pulsars known in each cluster. (Status: spring 2010).

Cluster	Obs-ID	Detector	Start Date	Exposure (s)
Terzan 5	654	ACIS-I	2000-07-29	5510[1]
	655	ACIS-I	2000-07-24	42161[1]
	3798	ACIS-S	2003-07-13	39344
47 Tucanea (NGC 104)	78	ACIS-I	2000-03-16	4050
	953	ACIS-I	2000-03-16	32080
	954	ACIS-I	2000-03-16	920
	955	ACIS-I	2000-03-16	32080
	956	ACIS-I	2000-03-17	4910
	2735	ACIS-S	2002-09-29	66100
	2736	ACIS-S	2002-09-30	66110
	2737	ACIS-S	2002-10-02	66110
	2738	ACIS-S	2002-10-11	69860
	3384	ACIS-S	2002-09-30	5580
	3385	ACIS-S	2002-10-01	5580
	3386	ACIS-S	2002-10-03	5830
	3387	ACIS-S	2002-10-11	6030
	5542	HRC-S	2005-12-19	50160
	5543	HRC-S	2005-12-20	51390
	5544	HRC-S	2005-12-21	50140
	5545	HRC-S	2005-12-23	51870
	5546	HRC-S	2005-12-27	50150
	6230	HRC-S	2005-12-28	49400
	6231	HRC-S	2005-12-29	47150
	6232	HRC-S	2005-12-31	44360
	6233	HRC-S	2006-01-02	97930
	6235	HRC-S	2006-01-04	50130
	6236	HRC-S	2006-01-05	51920
	6237	HRC-S	2005-12-24	50170
	6238	HRC-S	2005-12-25	48400
	6239	HRC-S	2006-01-06	50160
	6240	HRC-S	2006-01-08	49290
M28 (NGC 6626)	2683	ACIS-S	2002-09-09	14110
	2684	ACIS-S	2002-07-04	12746
	2685	ACIS-S	2002-08-04	13511
	9132	ACIS-S	2008-08-07	142260
	9133	ACIS-S	2008-08-10	54456
	2797	HRC-S	2002-11-08	49370
	6769	HRC-S	2006-05-27	41070
M15 (NGC 7078)	1903	HRC-I	2001-07-13	9096
	2412	HRC-I	2001-08-03	8821
	2413	HRC-I	2001-08-22	10790
	9584	HRC-I	2007-09-05	21445
NGC 6440	947	ACIS-S	2000-07-04	23279
	3799	ACIS-S	2003-06-27	24046

Table 1—Continued

Cluster	Obs-ID	Detector	Start Date	Exposure (s)
M62 (NGC 6266)	2677	ACIS-S	2002-05-12	62266
NGC 6752	948	ACIS-S	2000-05-12	29468
	6612	ACIS-S	2006-02-10	37967
M3 (NGC 5272)	4542	ACIS-S	2003-11-11	9932
	4543	ACIS-S	2004-05-09	10152
	4544	ACIS-S	2005-01-10	9441
M5 (NGC 5904)	2676	ACIS-S	2002-09-24	44656
M13 (NGC 6205)	5436	ACIS-S	2006-03-11	26799
	7290	ACIS-S	2006-03-09	27895
NGC 6441	721	HRC-I	2000-05-23	2290
M22 (NGC 6656)	5437	ACIS-S	2005-05-24	16020
M30 (NGC 7099)	2679	ACIS-S	2001-11-19	49435
NGC 6544	5435	ACIS-S	2005-07-20	16278
M4 (NGC 6121)	946	ACIS-S	2000-06-30	25816
	7446	ACIS-S	2007-07-06	46040
	7447	ACIS-S	2007-09-18	48540
M53 (NGC 5024)	6560	ACIS-S	2006-11-13	24565
M71 (NGC 6838)	5434	ACIS-S	2004-12-20	52446
NGC 6397	79	ACIS-I	2000-07-31	48343
	2668	ACIS-S	2002-05-13	28100
	2669	ACIS-S	2002-06-30	26660
	7460	ACIS-S	2007-07-16	147710
	7461	ACIS-S	2007-06-22	88898

Note. — [1] Data unusable because of a bright flaring source in the field of view.

Table 2. Distance, half-mass radius and column density of globular clusters which are known to host millisecond pulsars. The table is ordered top-down according to the number of radio millisecond pulsars known in each cluster. (Status: spring 2010).

Cluster	Distance (kpc)	r_{hm} (arcmin)	r_{core} (arcmin)	N_H (10^{21} cm^{-2})
Terzan 5	10.3	0.83	0.18	12.0
47 Tucanea (NGC 104)	4.5	2.79	0.44	0.1
M28 (NGC 6626)	5.6	1.56	0.24	2.2
M15 (NGC 7078)	10.3	1.06	0.07	0.6
NGC 6440	8.4	0.58	0.13	5.9
M62 (NGC 6266)	6.9	1.23	0.18	2.6
NGC 6752	4.0	2.34	0.17	0.2
M3 (NGC 5272)	10.4	1.12	0.55	0.06
M5 (NGC 5904)	7.5	2.11	0.42	0.2
M13 (NGC 6205)	7.7	1.49	0.78	0.1
NGC 6441	11.7	0.64	0.11	2.6
M22 (NGC 6656)	3.2	1.10	0.77	1.9
M30 (NGC 7099)	8.0	1.15	0.06	0.2
NGC 6544	2.7	1.77	0.05	4.1
M4 (NGC 6121)	2.2	3.65	0.83	2.0
M53 (NGC 5024)	17.8	1.11	0.36	0.1
M71 (NGC 6838)	4.0	1.65	0.63	1.4
NGC 6397	2.3	2.33	0.05	1.0

Note. — Globular cluster parameters from Harris (1996, update 2003). N_H from the optical reddening E(B-V) of the corresponding globular clusters.

Table 3. Period, spin-down energy and magnetic field strength of X-ray detected millisecond pulsars in globular clusters. (Status: spring 2010).

Cluster	Pulsar	P [a] 10^{-3} s	$\dot{E}$ ergs s^{-1}	$B_\perp$ 10^9 G	Binary[b]
47 Tucanea[c] (NGC 104)	J0024-7204C	5.7568	5×10^{32}	-	N
	J0024-7204D	5.3576	6.7×10^{33}	-	N
	J0024-7204E	3.5363	3.1×10^{34}	0.60	Y
	J0024-7204F	2.6236	4.1×10^{34}	0.42	N
	J0024-7204G	4.0404	$< 1.7 \times 10^{34}$	-	N
	J0024-7204H	3.2103	-	-	Y
	J0024-7204I	3.4850	$< 7.1 \times 10^{34}$	-	Y
	J0024-7204J	2.1006	3.2×10^{34}	-	Y
	J0024-7204L	4.3462	1.0×10^{34}	-	N
	J0024-7204M	3.6766	-	-	N
	J0024-7204N	3.0540	1.9×10^{34}	-	N
	J0024-7204O	2.6433	3.1×10^{34}	0.29	Y
	J0024-7204Q	4.0332	1.8×10^{34}	0.38	Y
	J0024-7204R	3.4805	2.8×10^{34}	-	Y
	J0024-7204S	2.8304	2.3×10^{34}	-	Y
	J0024-7204T	7.5885	1.1×10^{34}	1.51	Y
	J0024-7204U	4.3428	4.0×10^{34}	0.65	Y
	J0024-7204W	2.3523	-	-	Y
	J0024-7204Y	2.1967	4.8×10^{34}	-	Y
M28 (NGC 6626)	J1824-2452A	3.0543	2.2×10^{36}	2.25	N
	J1824-2452G	5.9091	3.4×10^{34}	1.07	Y
	J1824-2452H	4.6294	3.3×10^{34}	0.64	Y
NGC 6440	J1748-2021B	16.7601	2.8×10^{33}	2.45	Y
M62 (NGC 6266)	J1701-3006B	3.5939	3.0×10^{35}	1.17	Y
	J1701-3006C	3.8064	2.3×10^{34}	0.36	Y
NGC 6752	J1911-6000C	5.2773	5.9×10^{32}	0.11	N
	J1910-5959D	9.0353	5.2×10^{34}	3.08	N
M4 (NGC 6121)	B1620-26	11.0758	1.6×10^{33}	0.81	Y[d]
M71 (NGC 6838)	J1953+1846A	4.888	-	-	Y
Terzan 5	J1748-2446	-	-	-	-
NGC 6397	J1740-5340	3.6503	3.3×10^{34}	0.82	Y

Note. — a. From http://www.naic.edu/∼pfreire/GCpsr.html. b. Indicates whether the pulsar is in a binary system. c. $\dot{E}$ from Table 4 of Bogdanov et al. (2006). d. Long-orbit triple system with a white dwarf and a planet.

Table 4. Period, spin-down energy and magnetic field strength of X-ray non-detected millisecond pulsars in globular clusters.(Status: spring 2010).

Cluster	Pulsar	P [a] 10^{-3} s	$\dot{E}$ ergs s^{-1}	$B_{\perp}$ 10^{9} G	Binary[b]
NGC 6440	J1748-2021A	288.603	6.6×10^{32}	344	N
	J1748-2021C	6.2269	-	-	N
	J1748-2021D	13.4958	9.4×10^{33}	2.85	Y
	J1748-2021E	16.2640	2.9×10^{33}	2.28	N
	J1748-2021F	3.7936	-	-	Y
NGC 6441	J1750-3703A	111.608	1.6×10^{32}	25.4	Y
	J1750-3703B	6.0745	3.4×10^{33}	3.45	Y
	J1750-3703C	26.5687	-	-	N
	J1750-3703D	5.1399	1.4×10^{35}	16.1	N
NGC 6544	J1807-2459A	3.0595	-	-	Y
NGC 6752	J1910-5959B	8.3578	-	-	N
	J1910-5959E	4.5718	-	-	N
M13 (NGC 6205)	J1641+3627A	10.3775	-	-	N
M15 (NGC 7078)	B2127+11A	110.665	-	-	N
	B2127+11B	56.1330	2.1×10^{33}	23.4	N
	B2127+11C	30.5293	6.9×10^{33}	12.5	Y
	B2127+11D	4.8028	-	-	N
	B2127+11E	4.6514	7.0×10^{34}	0.92	N
	B2127+11F	4.0270	1.9×10^{34}	0.36	N
	B2127+11G	37.6602	1.5×10^{33}	8.78	N
	B2127+11H	6.7434	3.1×10^{33}	0.41	N
M28 (NGC 6626)	J1824-2452B	6.5466	-	< 0.4	N
	J1824-2452C	4.1583	9.3×10^{34}	< 1.2	Y
	J1824-2452D	79.8354	7.6×10^{34}	~ 91.0	Y
	J1824-2452E	5.4191	-	< 0.8	N
	J1824-2452F	2.4511	2.5×10^{34}	< 0.5	N
	J1824-2452I	3.9318	-	-	Y
	J1824-2452J	4.0397	-	< 0.6	Y
M30 (NGC 7099)	J2140-2310A	11.0193	-	-	Y
M3 (NGC 5272)	J1342+2822B	2.389	5.4×10^{34}	0.21	Y
	J1342+2822D	5.443	-	-	Y
M5 (NGC 5904)	B1516+02A	5.5536	9.5×10^{33}	0.48	N
	B1516+02B	7.9469	-	-	Y
M62 (NGC 6266)	J1701-3006A	5.2416	-	-	Y
Terzan 5	J1748-2446A	11.5632	-	-	Y
	J1748-2446C	8.4361	-	-	N

Note. — a. From http://www.naic.edu/∼pfreire/GCpsr.html. b. Indicates whether the pulsar is in a binary system.

Table 5. X-ray counterparts of globular cluster millisecond pulsars and their Chandra ACIS-S counting rates. (Status: spring 2010).

Globular Cluster	Pulsar	RA (J2000) h m s	Dec (J2000) d m s	δ RA arcsec	δ dec arcsec	Net count rate 10^{-4} cts/s	P_{coincide} %
47 Tucanae	J0024-7204C	00 23 50.364	-72 04 31.54	0.308	0.226	1.4 ± 0.3	0.018
	J0024-7204D	00 24 13.882	-72 04 43.84	0.242	0.213	3.4 ± 0.4	0.013
	J0024-7204E	00 24 11.107	-72 05 20.27	0.249	0.214	4.4 ± 0.4	0.014
	J0024-7204F	00 24 03.936	-72 04 42.50	0.231	0.212	6.1 ± 0.6	0.013
	J0024-7204G	00 24 07.943	-72 04 39.65	0.210	0.210	5.5 ± 0.5	0.011
	J0024-7204H	00 24 06.712	-72 04 06.95	0.256	0.214	2.7 ± 0.3	0.014
	J0024-7204I	00 24 07.936	-72 04 39.65	0.210	0.210	5.5 ± 0.5	0.011
	J0024-7204J	00 23 59.402	-72 03 58.93	0.262	0.219	1.2 ± 0.3	0.015
	J0024-7204L	00 24 03.754	-72 04 56.87	0.210	0.210	26.8 ± 0.6	0.011
	J0024-7204M	00 23 54.507	-72 05 30.77	0.286	0.219	2.2 ± 0.3	0.016
	J0024-7204N	00 24 09.224	-72 04 28.95	0.252	0.214	1.9 ± 0.3	0.013
	J0024-7204O	00 24 04.614	-72 04 53.83	0.210	0.210	9.4 ± 0.6	0.011
	J0024-7204Q	00 24 16.518	-72 04 25.26	0.256	0.214	2.5 ± 0.3	0.014
	J0024-7204R	00 24 07.551	-72 04 50.37	0.210	0.210	5.4 ± 0.4	0.011
	J0024-7204S	00 24 03.936	-72 04 42.50	0.231	0.212	6.1 ± 0.5	0.013
	J0024-7204T	00 24 08.552	-72 04 38.99	0.285	0.217	0.8 ± 0.2	0.016
	J0024-7204U	00 24 09.873	-72 03 59.71	0.246	0.213	3.1 ± 0.4	0.014
	J0024-7204W	00 24 06.035	-72 04 49.17	0.214^{b}	0.210^{b}	30.9 ± 1.2^{d}	0.012
	J0024-7204Y	00 24 01.454	-72 04 41.83	0.251^{b}	0.215^{b}	1.3 ± 0.3	0.014
M28 (NGC 6626)	J1824-2452A	18 24 32.007	-24 52 10.49	0.210	0.219	280.8 ± 5.8	0.024
	J1824-2452G	18 24 31.591	-24 52 17.49	0.226	0.341	2.9 ± 0.6	0.036
	J1824-2452H	18 24 31.591	-24 52 17.49	0.259	0.355	2.0 ± 0.7	0.027
NGC 6440	J1748-2021B	17 48 52.953	-20 21 38.86	0.214	0.287	variable^{a}	0.122
M62 (NGC 6266)	J1701-3006B	17 01 12.670	-30 06 49.04	0.225	0.228	9.0 ± 1.3	0.048
	J1701-3006C	17 01 12.867	-30 06 59.44	0.237	0.232	2.7 ± 0.9	0.051
NGC 6752	J1911-6000C	19 11 05.556	-60 00 59.68	0.297	0.248	3.3 ± 0.7	0.007
	J1910-5959D	19 10 52.417	-59 59 05.45	0.304	0.228	7.4 ± 1.1	0.007
M4 (NGC 6121)	B1620-26	16 23 38.222	-26 31 53.77	0.231	0.264	4.3 ± 1.1	0.004
M71 (NGC 6838)	J1953+1846A	19 53 46.424	18 47 04.91	0.231^{b}	0.238^{b}	5.6 ± 1.0	0.016
Terzan 5	J1748-2446	17 48 05.048	-24 46 41.10	0.220^{b}	0.219^{b}	30.5 ± 2.9^{c}	0.008
NGC 6397	J1740-5340	17 40 44.589	-53 40 40.90	0.218	0.235	variable^{a}	0.064

Note. — **a.)** The net counting rates for PSR J1748-2021B from observations in 2000-07-04 and 2003-06-27 are $(16.8 \pm 2.8) \times 10^{-4}$ cts/s and $(50.3 \pm 4.6) \times 10^{-4}$ cts/s, respectively. The net counting rates for PSR J1740-5340 from observations in 2000-07-31, 2002-05-13, 2002-06-30, 2007-06-22, 2007-07-16 are $(13.1 \pm 1.7) \times 10^{-4}$ cts/s, $(17.4 \pm 2.5) \times 10^{-4}$ cts/s, $(28.9 \pm 3.3) \times 10^{-4}$ cts/s, $(22.6 \pm 1.6) \times 10^{-4}$ cts/s and $(29.2 \pm 1.4) \times 10^{-4}$ cts/s, respectively. **b.)** Positional uncertainty of the X-ray counterpart only. Errors for the radio pulsar timing position are unpublished. **c.)** Based on observation ID. 3798 only. **d.)** Source exhibits variability at the binary period, count rate averaged over one orbit.

Table 6. Counting rate upper limits for X-ray emission from globular cluster millisecond pulsars.

Globular Cluster	Pulsar	RA (J2000) h m s	Dec (J2000) d m s	Counts^a	Exp. Time sec	3-σ UL^b 10^{-4} cts/s	$f_x^d/10^{-15}$ erg/s/cm^2
NGC 6440	J1748-2021A	17 48 52.689	-20 21 39.7	16.3	47325.1	3.9	6.77
	J1748-2021C	17 48 51.173	-20 21 53.81	2.2		2.5	4.34
	J1748-2021D	17 48 51.647	-20 21 07.41	2.2		2.5	4.34
	J1748-2021E	17 48 52.800	-20 21 29.38	1.1		2.1	3.65
	J1748-2021F	17 48 52.334	-20 21 39.33	1.1		2.3	3.99
NGC 6441	J1750-3703A	17 50 13.802	-37 03 10.95	2.2	2290.1	50.7	175.6
	J1750-3703B	17 50 12.177	-37 03 22.93	1.1		47.0	162.8
	J1750-3703C	17 50 13.454	-37 03 05.58	5.4		59.7	206.8
	J1750-3703D	17 50 13.097	-37 03 06.37	15.2		78.8	272.9
NGC 6544	J1807-2459A	18 07 20.36	-24 59 52.6	3.3	16277.6	7.6	11.02
NGC 6752	J1910-5959B	19 10 52.056	-59 59 00.86	14.1	67435.9	2.6	1.94
	J1910-5959E	19 10 52.157	-59 59 02.09	8.7		2.3	1.72
M13 (NGC 6205)	J1641+3627A	16 41 40.880	36 27 15.44	2.2	54693.8	2.1	1.53
M15 (NGC 7078)	B2127+11A	21 29 58.247	12 10 01.26	1029.35^c	30851.3	34.2	66.11
	B2127+11B	21 29 58.632	12 10 00.31	60.9		9.7	18.75
	B2127+11C	21 30 01.204	12 10 38.21	1.1		3.5	6.77
	B2127+11D	21 29 58.274	12 09 59.74	150.0^c		14.1	27.25
	B2127+11E	21 29 58.187	12 10 08.63	81.5		10.9	21.07
	B2127+11F	21 29 57.178	12 10 02.91	6.5		4.6	8.89
	B2127+11G	21 29 57.948	12 09 57.26	65.2		9.9	19.04
	B2127+11H	21 29 58.184	12 09 59.43	155.4^c		14.3	27.64
M28 (NGC 6626)	J1824-2452B	18 24 32.545	-24 52 04.29	19.6	196713.4	1.0	1.13
	J1824-2452C	18 24 33.089	-24 52 13.57	21.7		1.0	1.13
	J1824-2452D	18 24 31.812	-24 49 25.03	9.8		0.8	0.90
	J1824-2452E	18 24 32.900	-24 52 12.00	14.1		0.9	1.01
	J1824-2452F	18 24 32.733	-24 52 10.18	7.8		0.7	0.79
	J1824-2452I	18 24 32.192	-24 52 14.66	31.5		1.2	1.35
	J1824-2452J	18 24 32.422	-24 52 25.90	117.4^c		2.0	2.25
M30 (NGC 7099)	J2140-2310A	21 40 22.406	-23 10 48.79	6.5	49435.3	2.9	2.17
M3 (NGC 5272)	J1342+2822B	13 42 11.087	28 22 40.14	3.3	29525.9	4.2	3.02
	J1342+2822D	13 42 10.200	28 22 36.00	1.1		3.3	2.37
M5 (NGC 5904)	B1516+02A	15 18 33.318	02 05 27.55	2.2	44656.1	2.6	1.94
	B1516+02B	15 18 31.458	02 05 15.47	2.2		2.6	1.94
M62 (NGC 6266)	J1701-3006A	17 01 12.513	-30 06 30.13	4.3	62266.2	2.1	2.57
Terzan 5	J1748-2446A	17 48 02.255	-24 46 36.90	2.2	39343.8	3.0	7.88
	J1748-2446C	17 48 04.540	-24 46 36.00	3.3		3.1	8.14

Note. — [a]The total counts were extracted from a circle of 1 arcsecond radius (corresponding to 92% of the encircled energy) and then rescaled to the 100%. All counting rates are based on ACIS-S3 but for NGC 6441 and NGC 7078 (M15) which are based on HRC-I observations. [b]The 3-σ upper limits were computered by using $C = 0.5 \times (S/N)^2 + (S/N) \times \sqrt{cts + 0.25 \times (S/N)^2}$, in which $S/N = 3$ is the signal-to-noise ratio and cts the counts obtained at the pulsar position. [c]Upper limit dominated by a bright nearby source (cf. Figure 3). [d]Unabsorbed Flux in the 0.3 – 8.0 keV band.

Table 7. Ephemeris used in the timing analysis of PSR J1824-2452A, J0023-7204D, J0023-7204O and J0023-7204R.

Pulsar	Parameter	Value
J1824-2452A	MJD Range	50351-52610
	t_0 (MJD)	51468.0
	R.A. (J2000)	18h24m32.s008345
	DEC. (J2000)	–24d52m10.s758586
	$\phi(t_0)$	0.6316
	ν (s^{-1})	327.40564101150(1)
	$\dot{\nu}$ (10^{-12} s^{-2})	–0.1735080(1)
	$\ddot{\nu}$ (10^{-24}s^{-3})	0.66(1)
	Time System	DE405
J0024-7204D	MJD Range	48464-52357
	t_0 (MJD)	51600
	R.A. (J2000)	00h24m13.s87934(7)
	DEC. (J2000)	–72d04m43.s8405(3)
	ν (s^{-1})	186.651669856838(6)
	$\dot{\nu}$ (10^{-15} s^{-2})	0.1195(2)
	Time System	DE200
J0024-7204O	MJD Range	50683-52357
	t_0 (MJD)	51600
	R.A. (J2000)	00h24m04.s6512(1)
	DEC. (J2000)	–72d04m53.s7552(5)
	ν (s^{-1})	378.30878836037(3)
	Time System	DE200
	P_b(d)	0.1359743050(4)
	a_p/c sin(i)(s)	0.045151(2)
	T_{asc}(MJD)	51600.0757554(6)
	e	< 0.00016
J0024-7204R	MJD Range	
	t_0 (MJD)	51000
	R.A. (J2000)	00h24m07.s(6)
	DEC. (J2000)	–72d04m50.s(1)
	ν (s^{-1})	287.3181(0)
	Time System	DE200
	P_b(d)	0.066(2)
	a_p/c sin(i)(s)	0.33(4)
	T_{asc}(MJD)	50742.636(5)
	e	0.0

Note. — Ephemeris for J1824-2452A from Rots (2006) and references therein. t_0 corresponds to phase zeor. $\phi(t_0)$ is the phase of the main radio puls at t_0. Ephemeris of J0024-7204 D,O are from Freire et al. (2003) and for J0024-7204R from Camilo et al. (2000).

Table 8. Spectral parameters and luminosities of X-ray detected globular cluster millisecond pulsar counterparts.

Cluster	Pulsar	$N_H/10^{21}$ cm^{-2}	Model[a]	$\Gamma/kT(KeV)$	χ^2_ν (d.o.f)	log $L_{0.3\text{–}8\ \mathrm{keV}}$ [b] ergs s^{-1}	log $L_{0.1\text{–}2.4\ \mathrm{keV}}$ [b] ergs s^{-1}
47 Tucanae	J0024-7204C	0.1	BB	$0.24^{+0.05}_{-0.05}$	0.63(5)	$30.20^{+0.09}_{-0.12}$	$30.22^{+0.09}_{-0.10}$
	J0024-7204D	0.1	BB	$0.21^{+0.04}_{-0.03}$	0.89(11)	$30.40^{+0.13}_{-0.14}$	$30.44^{+0.11}_{-0.13}$
	J0024-7204E	0.1	BB	$0.16^{+0.02}_{-0.02}$	0.67(8)	$30.56^{+0.10}_{-0.10}$	$30.62^{+0.09}_{-0.07}$
	J0024-7204F/S	0.1	BB	$0.21^{+0.01}_{-0.01}$	1.27(19)	$30.87^{+0.09}_{-0.08}$	$30.91^{+0.10}_{-0.12}$
	J0024-7204G/I	0.1	BB	$0.24^{+0.04}_{-0.03}$	1.20(10)	$30.66^{+0.15}_{-0.12}$	$30.67^{+0.12}_{-0.14}$
	J0024-7204H	0.1	BB	$0.19^{+0.08}_{-0.05}$	1.19(7)	$30.31^{+0.21}_{-0.17}$	$30.35^{+0.18}_{-0.11}$
	J0024-7204J	0.1	BB+PL	$0.16^{+0.06\ c}_{-0.04}/0.61^{+0.55\ d}_{-0.26}$	0.72(10)	$31.06^{+0.27}_{-0.25}$	$30.70^{+0.29}_{-0.26}$
	J0024-7204L	0.1	BB+BB	$0.15^{+0.02}_{-0.02}/1.95^{+0.58}_{-0.51}$	1.47(21)	$31.60^{+0.28}_{-0.21}$	$31.17^{+0.30}_{-0.26}$
	J0024-7204M	0.1	BB	$0.14^{+0.04}_{-0.04}$	0.99(4)	$30.49^{+0.14}_{-0.11}$	$30.59^{+0.13}_{-0.13}$
	J0024-7204N	0.1	BB	$0.48^{+0.18}_{-0.16}$	1.03(7)	$30.32^{+0.17}_{-0.21}$	$30.20^{+0.28}_{-0.34}$
	J0024-7204O	0.1	BB+PL	$0.15^{+0.02\ c}_{-0.02}/1.33^{+0.24\ d}_{-0.22}$	1.06(10)	$31.34^{+0.31}_{-0.25}$	$31.08^{+0.29}_{-0.18}$
	J0024-7204Q	0.1	BB	$0.30^{+0.11}_{-0.08}$	1.19(6)	$30.14^{+0.17}_{-0.13}$	$30.14^{+0.19}_{-0.15}$
	J0024-7204R	0.1	BB+PL	$0.18^{+0.04\ c}_{-0.03}/1.51^{+0.67\ d}_{-0.65}$	1.71(16)	$31.44^{+0.27}_{-0.31}$	$31.28^{+0.27}_{-0.29}$
	J0024-7204T	0.1	BB	$0.26^{+0.09}_{-0.07}$	0.99(5)	$30.18^{+0.13}_{-0.15}$	$30.19^{+0.16}_{-0.18}$
	J0024-7204U	0.1	BB	$0.26^{+0.03}_{-0.06}$	1.00(10)	$30.36^{+0.08}_{-0.13}$	$30.37^{+0.09}_{-0.11}$
	J0024-7204W	0.1	BB+PL	$0.06^{+0.01\ c}_{-0.03}/1.72^{+0.16\ d}_{-0.17}$	0.97(19)	$31.39^{+0.12}_{-0.13}$	$31.39^{+0.11}_{-0.13}$
	J0024-7204Y	0.1	BB	$0.14^{+0.09}_{-0.05}$	1.73(5)	$30.34^{+0.16}_{-0.15}$	$30.43^{+0.15}_{-0.11}$
M28 (NGC 6626)	J1824-2452A	2.2 ± 0.2	PL	$1.13^{+0.03}_{-0.04}$	1.00(168)	$33.13^{+0.05}_{-0.03}$	$32.58^{+0.03}_{-0.03}$
	J1824-2452G	2.2	PL	$2.7^{+0.4}_{-0.5}$	0.83(12)	$31.14^{+0.07}_{-0.08}$	$31.49^{+0.29}_{-0.34}$
		2.2	BB	$0.3^{+0.1}_{-0.1}$	1.01(12)	$30.52^{+0.15}_{-0.24}$	$30.48^{+0.28}_{-0.36}$
	J1824-2452H	2.2	PL	$0.7^{+0.3}_{-0.4}$	0.77(13)	$31.20^{+0.36}_{-0.30}$	$30.53^{+0.18}_{-0.16}$
		2.2	BB	$1.1^{+0.3}_{-0.2}$	0.73(13)	$31.12^{+0.22}_{-0.18}$	$30.49^{+0.35}_{-0.20}$
NGC 6440	J1748-2021B (#947)	5.9	PL	$1.6^{+0.7}_{-0.5}$	1.49(7)	$32.32^{+0.46}_{-0.39}$	$32.10^{+0.44}_{-0.28}$

Table 8—Continued

Cluster	Pulsar	$N_H/10^{21}$ cm^{-2}	Model[a]	$\Gamma/kT(KeV)$	χ^2_ν (d.o.f)	log $L_{0.3-8\ \mathrm{keV}}$ [b] ergs s^{-1}	log $L_{0.1-2.4\ \mathrm{keV}}$ [b] ergs s^{-1}
	J1748-2021B (#3799)	5.9	PL	$1.4^{+0.2}_{-0.2}$	0.93(14)	$32.89^{+0.16}_{-0.18}$	$32.54^{+0.10}_{-0.12}$
M62 (NGC 6266)	J1701-3006B	2.6	PL	$2.1^{+0.3}_{-0.3}$	0.93(13)	$31.95^{+0.14}_{-0.13}$	$31.98^{+0.21}_{-0.18}$
		2.6	BB	$0.5^{+0.1}_{-0.1}$	1.22(13)	$31.69^{+0.38}_{-0.26}$	$30.52^{+0.43}_{-0.27}$
	J1701-3006C	2.6	PL	$1.7^{+0.9}_{-0.9}$	0.10(3)	$31.49^{+0.55}_{-0.37}$	$31.33^{+0.50}_{-0.32}$
NGC 6752	J1911-6000C	0.2	PL	$1.9^{+0.8}_{-0.8}$	0.98(4)	$30.70^{+0.39}_{-0.23}$	$30.62^{+0.45}_{-0.26}$
		0.2	BB	$0.3^{+0.1}_{-0.1}$	0.56(4)	$30.40^{+0.36}_{-0.32}$	$30.62^{+0.39}_{-0.30}$
	J1910-5959D	0.2	PL	$2.6^{+0.5}_{-0.4}$	0.70(8)	$30.99^{+0.11}_{-0.06}$	$31.26^{+0.35}_{-0.27}$
M4 (NGC 6121)	B1620-26	2.0	PL	$2.8^{+0.6}_{-0.5}$	1.05(8)	$30.58^{+0.09}_{-0.23}$	$31.01^{+0.31}_{-0.54}$
		2.0	BB	$0.4^{+0.1}_{-0.1}$	1.23(8)	$30.09^{+0.23}_{-0.28}$	$30.05^{+0.19}_{-0.34}$
M71 (NGC 6838)	J1953+1846A	1.4	PL	$1.9^{+0.5}_{-0.4}$	0.50(5)	$31.15^{+0.36}_{-0.30}$	$31.10^{+0.31}_{-0.54}$
Terzan 5	J1748-2446	12.0	PL	$1.0^{+0.3}_{-0.2}$	0.44(10)	$33.01^{+0.19}_{-0.19}$	$32.51^{+0.19}_{-0.13}$
		12.0	BB	$1.0^{+0.2}_{-0.1}$	0.70(10)	$32.83^{+0.17}_{-0.22}$	$32.27^{+0.21}_{-0.25}$
NGC 6397	J1740-5340 (#79)	1.0	PL	$1.8^{+0.3}_{-0.3}$	0.75/6	$31.06^{+0.32}_{-0.27}$	$30.95^{+0.31}_{-0.41}$
		1.0	BB	$0.6^{+0.1}_{-0.1}$	0.67/6	$30.82^{+0.35}_{-0.38}$	$30.63^{+0.29}_{-0.33}$
	J1740-5340 (#2668)	1.0	PL	$1.5^{+0.3}_{-0.3}$	0.75/8	$31.08^{+0.30}_{-0.44}$	$30.81^{+0.32}_{-0.38}$
		1.0	BB	$0.6^{+0.1}_{-0.1}$	0.75/8	$30.77^{+0.37}_{-0.28}$	$30.59^{+0.19}_{-0.27}$
	J1740-5340 (#2669)	1.0	PL	$1.5^{+0.2}_{-0.2}$	1.14/8	$31.20^{+0.17}_{-0.25}$	$30.92^{+0.16}_{-0.22}$
		1.0	BB	$0.7^{+0.1}_{-0.1}$	1.28/8	$30.97^{+0.29}_{-0.20}$	$30.70^{+0.22}_{-0.31}$
	J1740-5340 (#7460)	$0.9^{+1.0}_{-0.4}$ [e]	PL	$1.4^{+0.1}_{-0.1}$	0.97/11	$30.95^{+0.15}_{-0.14}$	$30.99^{+0.12}_{-0.09}$
	J1740-5340 (#7461)	$\lesssim 1.0$ [e]	PL	$1.7^{+0.4}_{-0.2}$	1.06/5	$30.95^{+0.26}_{-0.20}$	$30.99^{+0.13}_{-0.15}$

Note. — Note: The meaning of the columns are as follows: Cols. 1 &2 list the cluster and pulsar name, Cols. 3 to 5 list the hydrogen column density, the spectral model and the best-fitted photon index or blackbody temperature, depending on the fitted model. Col.6 lists the reduced χ^2 together with the degrees of freedom given in brackets. Cols. 7 & 8 list the unabsorbed X-ray luminosity in the $0.3-8.0$ and $0.1-2.4$ keV energy ranges, respectively. Quoted errors indicate the 68% confidence level for one parameter of interest.

[a] PL = power-law; BB = blackbody

[b] Unabsorbed X-ray luminosities are computed at the distance of the GC (cf. Table 3 and Harris 1996, updated 2003).

[c] The value indicates the blackbody temperature in the unit of keV.

[d] The value indicates the photon index inferred from the power-law model.

[e] The best-fitted N_H values are consistent with the values of $\sim 1.03 \times 10^{21}\mathrm{cm}^{-2}$ which is inferred from the optical reddening of NGC 6397.